Modelling preferential flow induced by dynamic changes of desiccation cracks
A comparative numerical study

Luo, Yi; Zhang, Jiaming; Zhou, Zhi; Victor, Chikhotkin

DOI
10.1016/j.geoderma.2023.116471

Publication date
2023

Document Version
Final published version

Published in
Geoderma

Geoderma 433 (2023) 116471

Contents lists available at ScienceDirect

Geoderma

journal homepage: www.elsevier.com/locate/geoderma

Modelling preferential flow induced by dynamic changes of desiccation cracks: A comparative numerical study

Yi Luo [a,b], Jiaming Zhang [a], Zhi Zhou [c,*], Chikhotkin Victor [a]

[a] Faculty of Engineering, China University of Geosciences (Wuhan), 388 Lumo Avenue, Wuhan 430074, China
[b] Water Resources Section, Faculty of Civil Engineering and Geosciences, Delft University of Technology, Stevinweg 1, P.O. Box 5048, 2600 GA Delft, the Netherlands
[c] Department of Engineering Management, Hubei University of Economics, No.8 Yangqiaohu Road, Wuhan 430205, China

ARTICLE INFO

Keywords:
Desiccation cracks
Preferential flow
Dynamic changes
Dual-permeability model
Numerical experiments

ABSTRACT

Quantitative investigation on the preferential flow induced by desiccation cracks (PF-DC) remains a great challenge due to the soil shrinking-swelling behavior. This work presents a series of comparative numerical studies to investigate the accuracy and substitutability of different models in simulating the water flux, hydrological response and crack evolution induced by PF-DC. As a comparative study, an effective dynamic dual-permeability model (DDPM) we recently developed and validated was regarded as a benchmark model. Three numerical experiments were conducted to (i) compare the difference among the single-domain model (SDM), rigid dual-permeability model (RDPM) and DDPM; (ii) test the sensitivity of the DDPM to the shrinking-swelling parameters; (iii) test the rationality of a "lighter" dynamic DPM (LDPM) only considering the proportion changes of each domain while neglecting the variation of hydraulic properties. The results showed that compared to the DDPM, the SDM overestimated the water content under low-rainfall intensity while underestimating the water content under high-intensity rainfall and failed to capture the early increase of water content in deep soils induced by PF-DC. The RDPM greatly overestimated the total water content and water storage capacity of the crack domain, which was not suggested to be used in the surface runoff or flood forecast. The DDPM is overall not sensitive to the shrinking-swelling parameters, indicative of relatively loose accuracy requirements in measuring the soil shrinking-swelling parameters. The LDPM can be a tentative alternative option for the DDPM, but it is better not to use it to evaluate the surface runoff or use it under long-term extreme drought. In conclusion, the prediction errors without considering crack evolution and variation of hydraulic properties of each domain (RDPM) are the highest, then followed by the only considering crack evolution (LDPM) and uncertainties of shrinking-swelling parameters.

1. Introduction

Desiccation cracks are prevalent in cracked clay soils (Davidson, 1984; Weiler, 2005), which often serve as preferred pathways leading water to rapidly infiltrate into subsoils as preferential flow (Beven and Germann, 1982; Greve et al., 2010). The preferential flow induced by desiccation cracks (PF-DC) has proven to be an important hydrological process that could lead to geotechnical engineering and ecological environment problems, such as dike and slope instability (Jamalinia et al., 2020; Zhang et al., 2021a; Zhang et al., 2021b), shallow landslides (Bogaard and Greco, 2015; Caris and Van Asch, 1991), groundwater pollution (Chen et al., 2002; Mooney and Morris, 2008) and reduction of irrigation efficiency (Greve et al., 2010; Smith et al., 2005). Under the current background of increasing incidents of extreme droughts and precipitation due to climate change (Chaduvula et al., 2022; Coumou and Rahmstorf, 2012), the dry spells will enlarge the desiccation cracks and facilitates the PF-DC during subsequent heavy rainfall. The negative consequences of the PF-DC will be exacerbated. However, as the complex spatiotemporal variability of the desiccation cracks with moisture content, the PF-DC is not well understood due to a lack of effective simulation methods.

As a pioneer on soil desiccation cracking, Tang et al. (2011) conducted systematic study and revealed that the desiccation cracks have unique dynamic features in their volume, depth and connectivity with soil moisture content (Tian et al., 2022; Xu et al., 2022; Zeng et al., 2021), causing great challenges in modeling the evolution of desiccation cracks. Regarding the existing forms of the soil cracks in the numerical

* Corresponding author.
E-mail address: zhouzhiab@cug.edu.cn (Z. Zhou).

https://doi.org/10.1016/j.geoderma.2023.116471
Received 18 September 2022; Received in revised form 30 March 2023; Accepted 6 April 2023
Available online 13 April 2023

Nomenclature

PF-DC	Preferential flow induced by desiccation cracks
DEM	Discrete element method
FEM	Finite element method
EM	Static explicit method to model PF-DC
SDM	Single-domain model without considering preferential flow
RDPM	Rigid dual-permeability model with fixed crack ratio and hydraulic conductivity
DDPM	Dynamic DPM with changing crack ratio and hydraulic conductivity
LDPM	Lighter DDPM only considering changes of crack ratio
θ	Total water content (combined matrix and crack domains), m^3m^{-3}
θ_m	Volumetric water content of the matrix domain, m^3m^{-3}
θ_c	Volumetric water content of the crack domain, m^3m^{-3}
$\theta_{m,s}$	Saturated volumetric water content of the matrix domain, m^3m^{-3}
$\theta_{m,r}$	Residual volumetric water content of the matrix domain, m^3m^{-3}
$\theta_{c,s}$	Saturated volumetric water content of the crack domain, m^3m^{-3}
$\theta_{c,r}$	Residual volumetric water content of the crack domain, m^3m^{-3}
$S_{e,m}$	Saturation degree of the matrix domain, m^3m^{-3}
$S_{e,c}$	Saturation degree of the crack domain, m^3m^{-3}
α_m	Parameter for the van Genuchten water retention curve of the matrix domain, 1/m
n_m	Parameter for the van Genuchten water retention curve of the matrix domain, 1/m
m_m	Parameter for the van Genuchten water retention curve of the matrix domain, 1/m
α_c	Parameter for the van Genuchten water retention curve of the crack domain, 1/m
n_c	Parameter for the van Genuchten water retention curve of the crack domain, 1/m
m_c	Parameter for the van Genuchten water retention curve of the crack domain, 1/m
h_m	Pressure head of the matrix domain, m
h_c	Pressure head of the crack domain, m
C_c	Specific water capacity of the crack domain which is defined as $d\theta_c/dh_c$, 1/m
C_m	Specific water capacity of the matrix domain which is defined as $d\theta_m/dh_m$, 1/m
K_s	Total transient saturated hydraulic conductivity of the soil (combined matrix and crack domains), m/s
K_c	Transient hydraulic conductivity of the crack domain, m/s
$K_{c,s}$	Saturated hydraulic conductivity of the crack domain, m/s
$K_{c,\max}$	The maximum crack hydraulic conductivity when the crack reaches its maximum crack aperture, m/s
$K_{c,\min}$	The minimum crack hydraulic conductivity when the crack reaches its minimum crack aperture, m/s
$K_{c,r}$	Relative hydraulic conductivity of the crack domain, m^3m^{-3}
K_m	Transient hydraulic conductivity of the matrix domain, m/s
$K_{m,s}$	Saturated hydraulic conductivity of the matrix domain, m/s
$K_{m,\max}$	The maximum matrix hydraulic conductivity prior to soil shrinkage, m/s
$K_{m,r}$	Relative hydraulic conductivity of the matrix domain, m^3m^{-3}
K_a	Hydraulic conductivity between the matrix and crack domains, m/s
$K_{a_{\min}}$	An improved hydraulic conductivity between the matrix and crack domains reformulated by Gerke et al. (2013), m/s
Γ_w	Water exchange term between the crack and matrix domains, 1/s
w_c	Crack ratio, which is defined as volumetric ratio between the crack domain and the overall soil volume, m^3m^{-3}
$w_{j,\max}$	The maximum average crack aperture measured in the experiment, m
w_m	Volumetric ratio between the matrix domain and the overall soil volume, m^3m^{-3}
α_w	Effective water transfer coefficient, $1/m^2$
β	A dimensionless factor which depends on the shape of the soil matrix and is set as 3
γ_w	A dimensionless "scaling" coefficient with a suggested value of 0.4
a	A scaling factor approximately equaling to the half width of the average block size
ε	Total soil porosity (combined matrix and crack domains), which is defined as total pore volume divided by total soil volume, m^3m^{-3}
ε_m	Effective porosity of the matrix domain, which is defined as pore volume in matrix divided by the volume of matrix domain
ε_c	Effective porosity of the matrix domain, which is defined as pore volume in matrix divided by the volume of crack domain
i	Total boundary flow rate (combined matrix and crack domains), m/s
i_m	Transient boundary flow rate of the matrix domain, m/s
i_c	Transient boundary flow rate of the crack domain, m/s
I_m	Cumulative boundary flow rate of the matrix domain, m
I_c	Cumulative boundary flow rate of the crack domain, m
d_m	Transient bottom drainage rate of the matrix domain, m/s
D_m	Cumulative bottom drainage rate of the matrix domain, m
r	Rainfall intensity, m/s
PE	Potential evaporation rate, m/s
$\phi_{\max}$	The maximum porosity) of a soil core prior to soil shrinkage. m^3m^{-3}
$\phi_{\min}$	The minimum porosity of the matrix domain, m^3m^{-3}
ϕ_{matrix}	Porosity of the matrix domain, which is defined as pore volume in matrix divided by the total soil volume, m^3m^{-3}
ϕ_{crack}	Porosity of the crack domain, which is defined as pore volume in crack domain divided by the total soil volume, m^3m^{-3}
p	Functional shape parameters of the soil shrinkage curve
q	Functional shape parameters of the soil shrinkage curve

model, current simulation methods can be basically classified as explicit and implicit methods. The explicit method visualizes desiccation cracks by simulating the particle (or matrix blocks) contraction using the discrete element method (DEM) (Sima et al., 2014; Tang et al., 2021; Tran et al., 2020) or finite element method (FEM) (Sánchez et al., 2014; Shin and Santamarina, 2011; Vo et al., 2017). These kinds of dynamic explicit methods are often used to simulate crack evolution and crack morphology during evaporation at small scales. However, they are rarely adopted to model the water infiltration and redistribution under long-term wetting–drying cycles for their intrinsic shortcomings in simulating the complex hydrological process (e.g. lack of proper constitutive hydrological models). Consequently, an alternative static

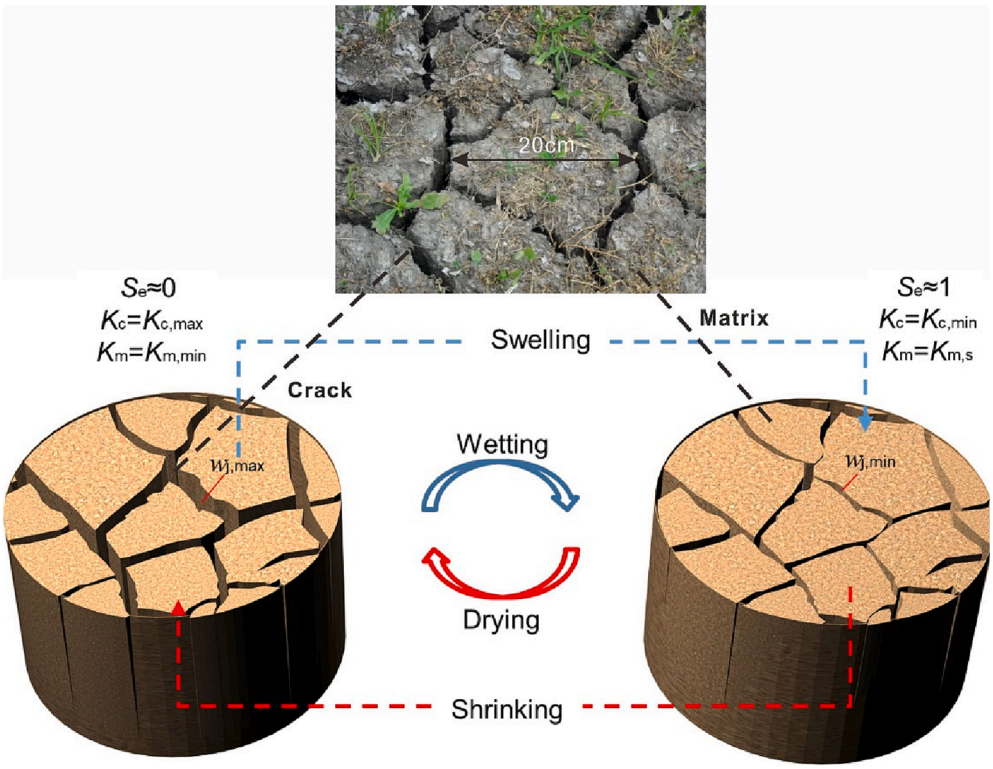

Fig. 1. Illustration of the model concept.

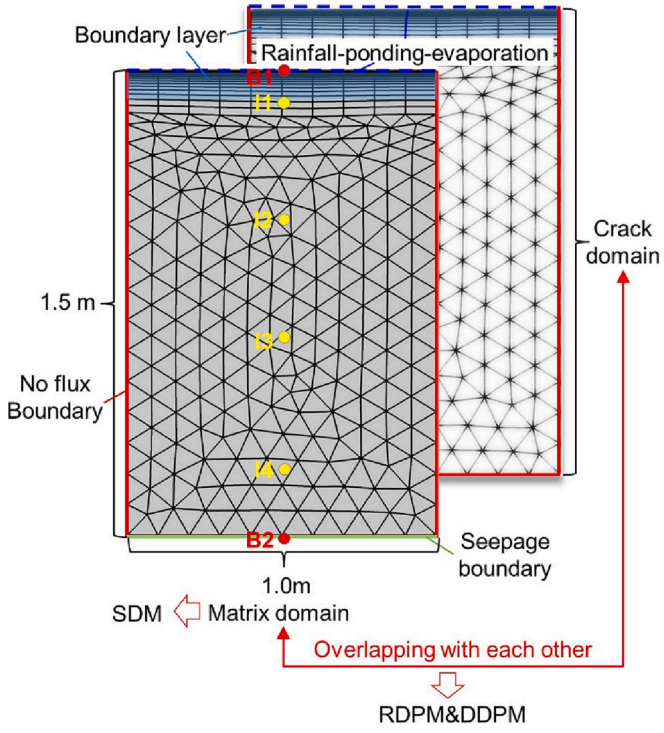

Fig. 2. Set-up of the numerical model.

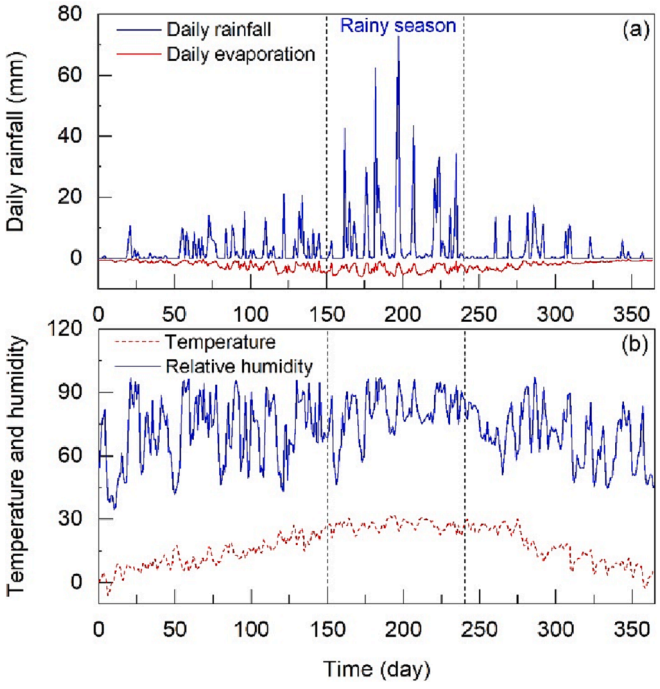

Fig. 3. Boundary atmospheric conditions.

explicit method (EM), which usually defines the details involving the geometry, spatial distribution and hydrological properties of each crack, was widely used to simulate hydrological process induced by soil cracks building on FEM (Khan et al., 2017; Pei et al., 2020; Xie et al., 2020). Nevertheless, the EM always assumes the cracks are spatiotemporally fixed and thus is defective in describing the dynamic features of desiccation cracks. Meanwhile, the EM is computationally unfeasible when simulating network-distributed desiccation cracks (Aguilar-López et al., 2020), particularly at a large scale (i.e. slope scale). While some coupled FEM-DEM methods are developed (Gui et al., 2016; Hirobe and Oguni, 2016; Wijerathne et al., 2009), they are over-parametric and complex to apply due to the computational burden.

The implicit method often assumes the soil pore system can be

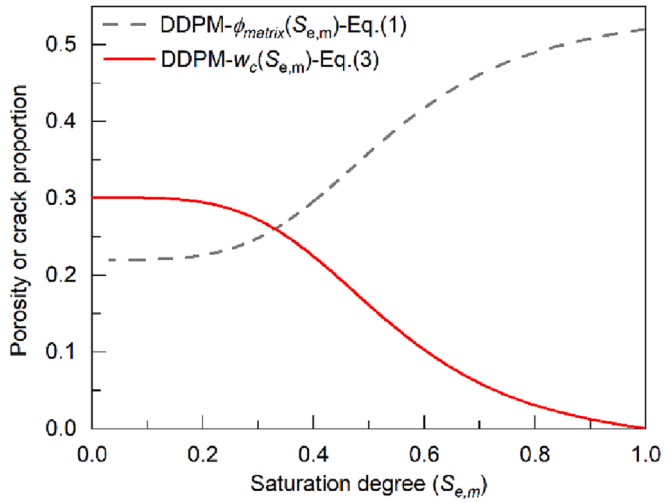

Fig. 4. Variation of matrix porosity and crack proportion with the matrix saturation degree.

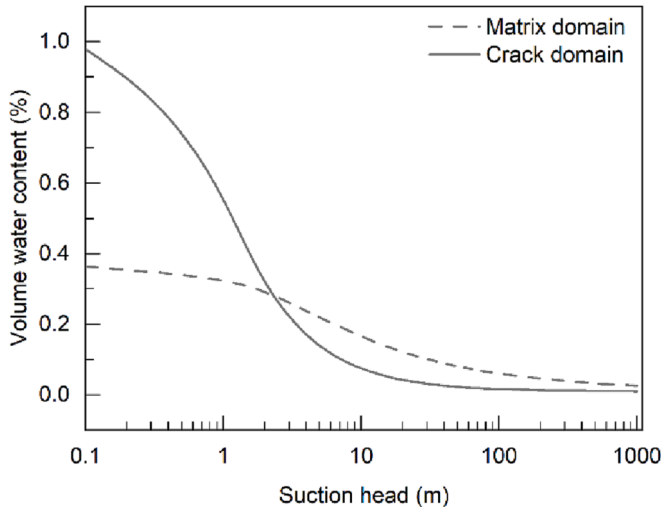

Fig. 5. Soil water retention curves of the matrix and crack domains.

represented as multi overlapping interacting regions, one which represents the matrix domain with micropores and the others represent domains with different kinds of *meso*-macro pores (i.e. desiccation cracks and biological holes). These kinds of models may be not suitable for a sole dominant crack in soils but can well simulate pervasive macro pores in the soils, such as desiccation cracks or earthworm holes. The most well-known model is the classical/rigid dual-permeability model (RDPM) which used Richards equation (Aguilar-López et al., 2020; Gerke and van Genuchten, 1993; Gerke and Maximilian Köhne, 2004; Larsbo and Jarvis, 2003; Šimůnek et al., 2003) or the Green-Ampt model (Davidson, 1984; Stewart, 2019) building on Darcy's flow law to simulate water flow both in the crack and matrix domains. Despite some critics on the Richards-equation-based RDPM (Nimmo, 2010; Nimmo et al., 2021), it has still been widely accepted and used in simulating preferential flow in soils due to its easily available parameters, reasonably satisfactory prediction to the measurements and high computation efficiency (Jarvis et al., 2016). However, the RDPM assumes the crack volume and hydrological properties of each domain keep spatiotemporally constant, which is unfeasible to capture the dynamic features of PF-DC (Luo et al., 2023).

In our recent study (Luo et al., 2023), a new and effective dynamic preferential flow model (DDPM) based on the dual-permeability concept

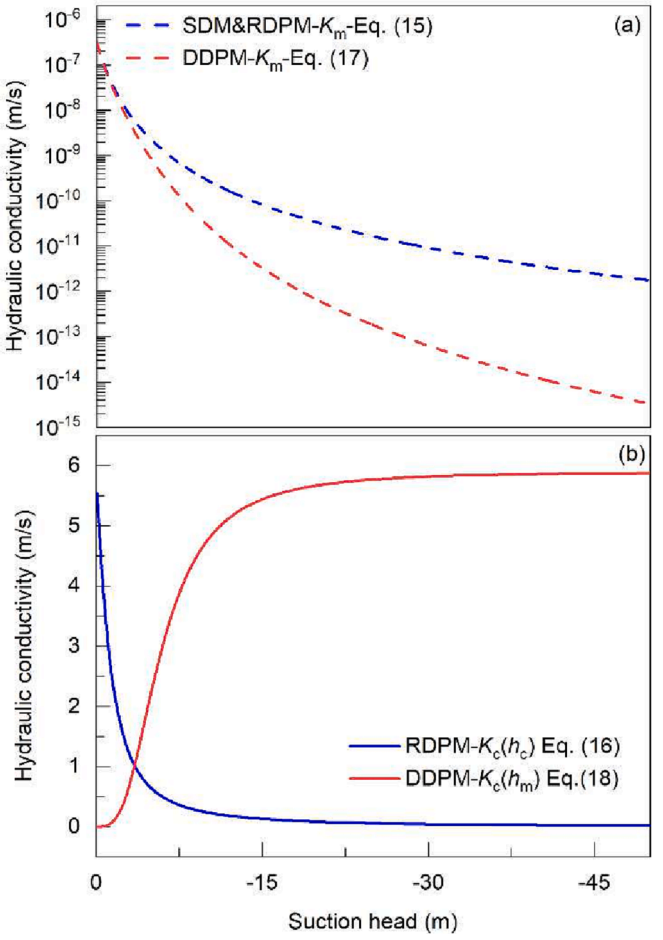

Fig. 6. Comparative curves of K_m and K_c in the SDM, RDPM and DDPM. (a) K_m in the SDM, RDPM and DDPM; (b) K_c in the RDPM and DDPM.

was proposed to account for the PF-DC controlled by the soil shrinking-swelling behavior. The model has a physically-consistent definition. It remedies the shortcomings of the RDPM and other dynamic preferential flow models in defining the dynamic changes of desiccation cracks (Coppola et al., 2012; Coppola et al., 2015) and hydraulic properties of each domain and interface (Bagnall et al., 2019; Jamalinia et al., 2020; Kroes et al., 2000; Lepore et al., 2009; Luo et al., 2021; Stewart, 2018). Most importantly, the model showed good correspondence to the soil column (0.5 m by 0.5 m) infiltration experiment (Luo et al., 2023). Nevertheless, due to the small crack depth and experimental scale, the differences among the single-domain model (SDM), RDPM and DDPM are not significant enough to stress the effects of PF-DC on the soil infiltration process under atmospheric environment. Additionally, in reality, when the soil shrinking-swelling parameters are absent or the simplicity and robustness of the model strike the high priority (Lepore et al., 2009), one may comprise to substitute the DDPM as a 'lighter' (or simplified) dynamic dual-permeability model or even rigid ones to simulate the infiltration process induced by PF-DC. It is necessary to examine the substitutability of these model to the DDPM. Also, considering the possible inaccurate shrinking-swelling parameters, the sensitivity of the DDPM to the shrinking parameters needs further study.

The objective of this work is to investigate the accuracy and substitutability of different models in simulating the water flux, hydrological response and crack evolution induced by PF-DC. Under one-year atmospheric conditions, three numerical experiments were conducted to (i) compare the difference among the single-domain model (SDM), rigid dual-permeability model (RDPM) and dynamic dual-permeability model (DDPM); (ii) investigate the sensitivity of the DDPM to the shrinking-

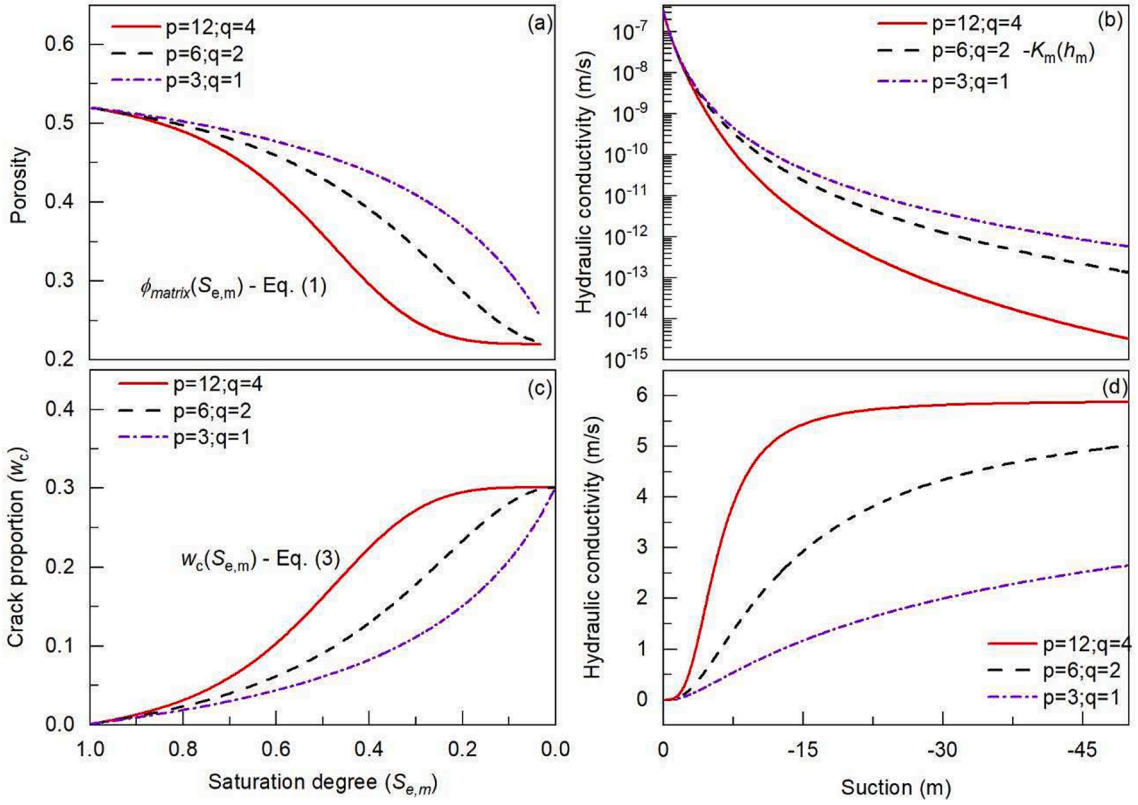

Fig. 7. Variation of porosity and hydraulic conductivity of each domain in DDPM with different shrinking-swelling parameters. (a) and (c) refer to the matrix porosity and crack proportion, respectively; (b) and (d) refer to the matrix and crack hydraulic conductivity, respectively.

Table 1
Fixed parameters for all models.

Model	Parameter	Units	Value
SDM RDPM	$\theta_{m,s}$	(−)	0.366
DDPM	$\theta_{m,r}$	(−)	0.01
LDPM	α_m	(1/m)	0.5
	n_m	(−)	1.5
	$K_{m,max}$	(m/s)	5.56×10^{-7}
RDPM	$\theta_{c,s}$	(−)	0.99
DDPM	$\theta_{c,r}$	(−)	0.01
LDPM	α_c	(1/m)	1.5
	n_c	(−)	2
	$K_{c,max}$	(m/s)	5.9
	K_a	(m/s)	K_{amin}
	β	(−)	3
	γ_w	(−)	0.4
	a	(mm)	100
DDPM	ϕ_{max}	(−)	0.52
LDPM	ϕ_{min}	(−)	0.22

Table 2
Description and values used for different experiments.

Experiment	Description	$K_{m,s}$	$K_{c,s}$	p	q	w_m	w_c
1.1	DDPM	Eq. (2)	Eq. (4)	12	4	1- Eq. (3)	Eq. (3)
1.2	SDM	$K_{m,max}$	–	–	–	–	–
1.3	RDPM	$K_{m,max}$	$K_{c,max}$	–	–	0.794	0.206
2.1	DDPM	Eq. (2)	Eq. (4)	3	1	1- Eq. (3)	Eq. (3)
2.2	DDPM	Eq. (2)	Eq. (4)	6	2	1- Eq. (3)	Eq. (3)
2.3	DDPM	Eq. (2)	Eq. (4)	12	4	1- Eq. (3)	Eq. (3)
3.1	LDPM	$K_{m,max}$	$K_{c,max}$	12	4	1- Eq. (3)	Eq. (3)
3.2	DDPM	Eq. (2)	Eq. (4)	12	4	1- Eq. (3)	Eq. (3)

swelling parameters; (iii) test the rationality of a "lighter" dynamic DPM, where the soil shrinkage only induces a change in the crack volume while has no influence on the hydraulic properties of the two domains.

2. Model description

The basic idea of our dynamic preferential flow model (DDPM, Luo et al. (2023)) is to incorporate a soil shrinking-swelling model into the classical/rigid dual-permeability model (RDPM). The shrinking-swelling model proposed by Stewart et al. (2016a); Stewart et al. (2016b), including physically-consistent functions in describing the variation of both porosity and hydraulic conductivity in the crack and matrix domains, inspired us to develop the DDPM.

2.1. Variation of porosity and hydraulic conductivity

As shown in Fig. 1, the shrinking-swelling model can be briefly summarized as follow.

For the matrix domain, Stewart et al. (2016a); Stewart et al. (2016b) proposed Eqs. (1) and (2) to describe the variation of porosity and saturated hydraulic conductivity. Both of them are functions involving the saturated degree of the matrix domain. Here, the subsidence induced by soil shrinkage is neglected in our study, indicating that the reduction of matrix porosity during soil shrinkage all transfers to the crack space.

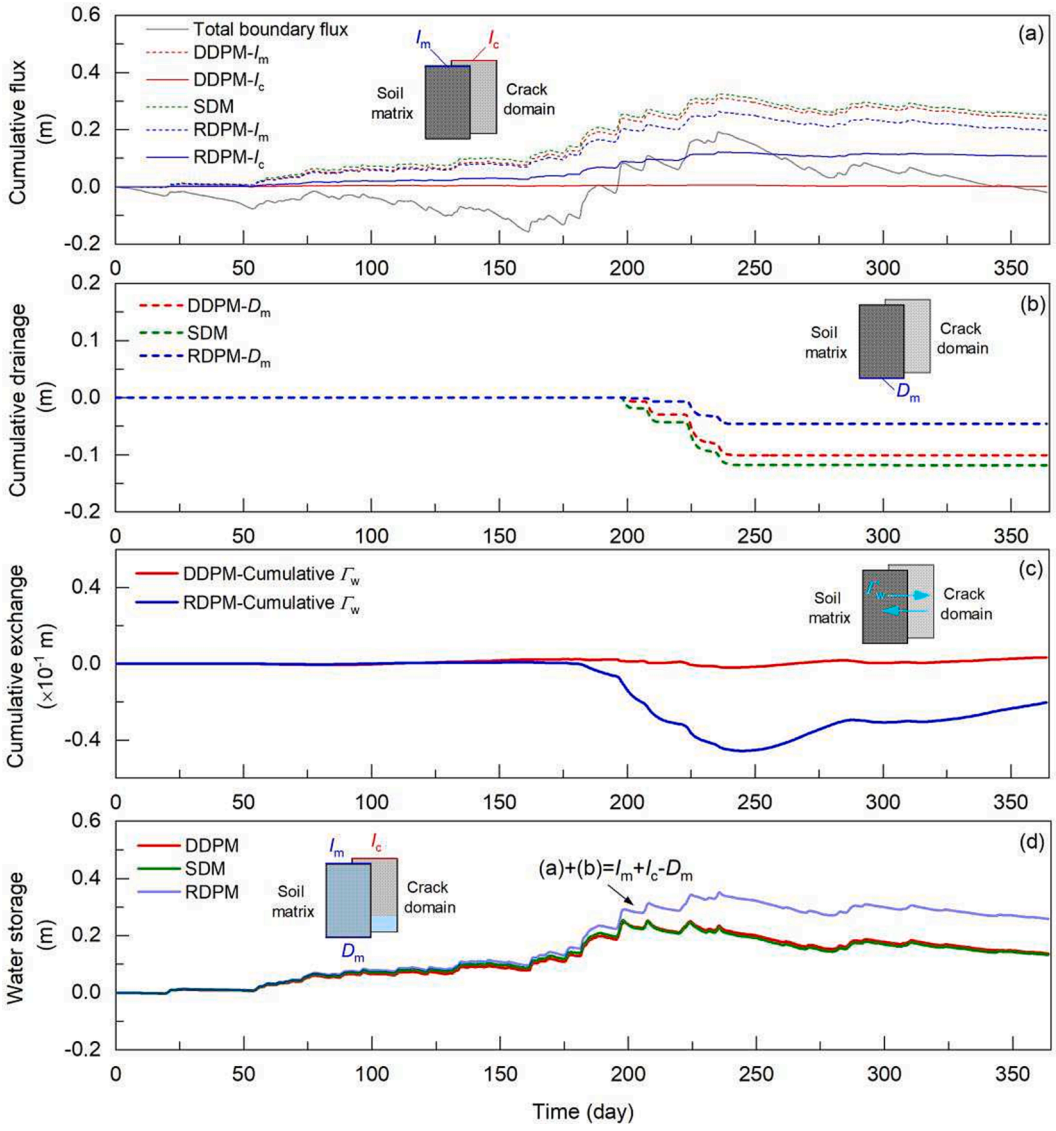

Fig. 8. Cumulative boundary water flux obtained from point B1 and B2 and corresponding water balance of the DDPM, SDM and RDPM. (a) cumulative boundary flux of the three models; (b) cumulative drainage flux of the three models (c) cumulative total water exchange of the DDPM and RDPM; (d) temporal evolution of the water storage in the three models, which equals to the difference between the cumulative inlet flux and cumulative outlet flux.

$$\phi_{matrix}(S_{e,m}) = (\phi_{\max} - \phi_{\min})\left(\frac{p+1}{p+S_{e,m}^{-q}}\right) + \phi_{\min} \quad (1)$$

$$K_{m,s}(S_{e,m}) = K_{m,\max}\left(\frac{p+1}{p+S_{e,m}^{-q}}\right) \quad (2)$$

where ϕ_{matrix} refers to the matrix porosity defined as pore volume in the matrix domain divided by the soil total volume; $\phi_{\max}$, $\phi_{\min}$, p and q are shrinkage parameters that can be determined by soil shrinkage test.

$\phi_{\max}$- the maximum porosity of a soil core prior to shrinkage and thus also represents the total porosity;
$\phi_{\min}$- the minimum porosity of the matrix domain;
p and q - functional shape parameters;
$S_{e,m}$- saturation degree of the matrix domain;
$K_{m,s}$- the saturated hydraulic conductivity of the matrix domain;
$K_{m,\max}$- the maximum saturated hydraulic conductivity of the matrix domain (at $S_{e,m} = 1$).

For the crack domain, variation of the crack proportion and its saturated hydraulic conductivity can be described by follow equations.

$$w_c(S_{e,m}) = (\phi_{\max} - \phi_{\min})\left(\frac{1 - S_{e,m}^{q}}{1 + pS_{e,m}^{q}}\right) w_{c,\min} \quad (3)$$

$$K_{c,s}(S_{e,m}) = K_{c,\max}\left(\frac{1 - S_{e,m}^{q}}{1 + pS_{e,m}^{q}}\right)^2 + K_{c,\min} \quad (4)$$

where w_c refers to the crack proportion defined as the crack volume divided by the soil total volume;

$K_{c,s}$- the saturated hydraulic conductivity of the crack domain;
$K_{c,\max}$- the maximum saturated hydraulic conductivity of the crack domain (at $S_{e,m} \approx 0$);
$w_{c,\min}$- the minimum crack proportion due to incomplete crack closure process (Coppola et al., 2012; Coppola et al., 2015; Luo et al., 2023);
$K_{c,\min}$- the minimum saturated hydraulic conductivity of the crack domain corresponds to the $w_{c,\min}$ (at $S_{e,m} \approx 1$).

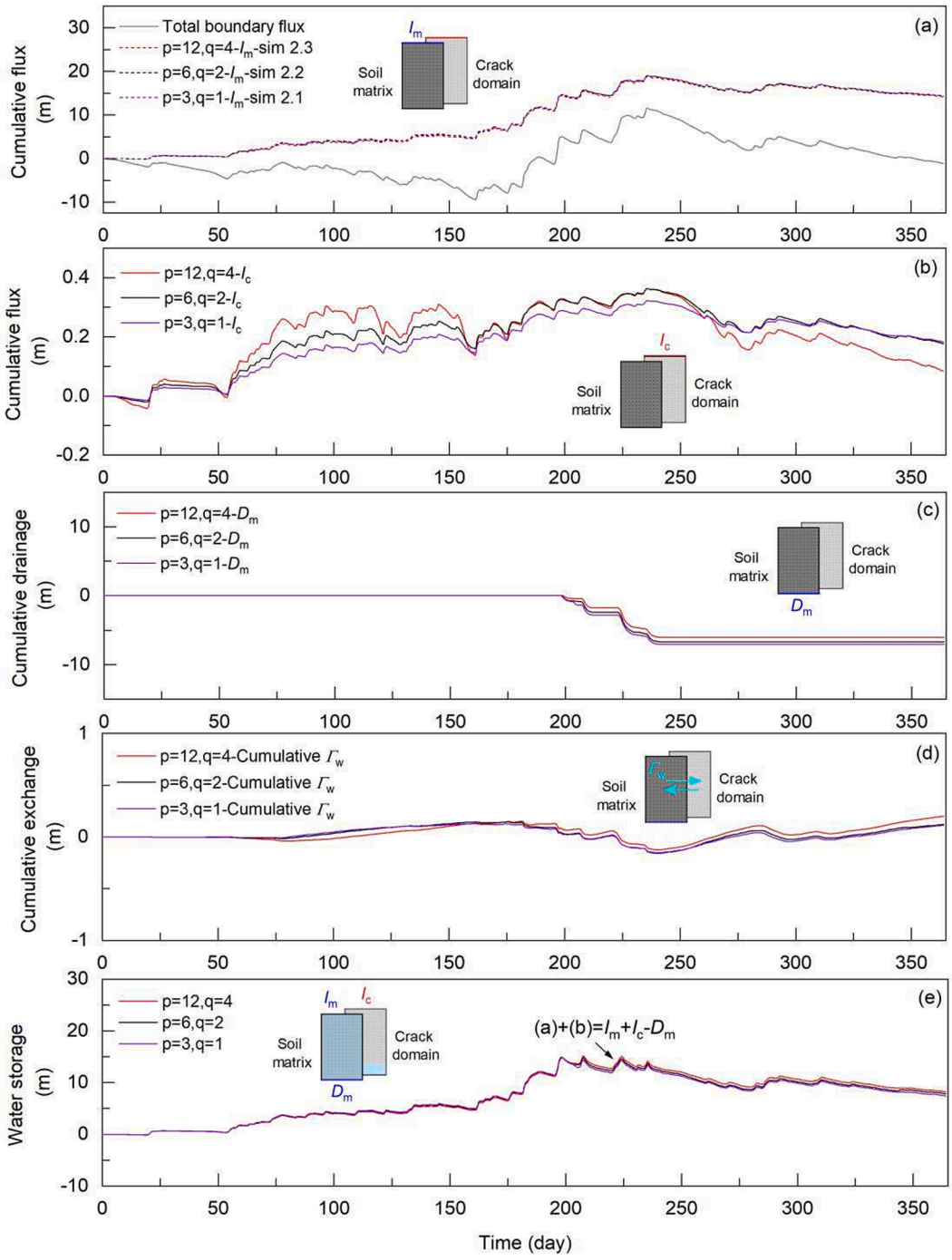

Fig. 9. Cumulative boundary water flux obtained from point B1 and B2 and corresponding water balance in the sim 2.1, sim 2.2 and sim 2.3. (a) cumulative matrix flux; (b) cumulative preferential flow flux; (c) cumulative drainage flux; (d) cumulative total water exchange; (e) the temporal evolution of the water storage.

Overall, Eqs. (1)–(4) are the core equations in the SSM. More details can be found in Luo et al. (2023).

2.2. Rigid dual-permeability model (RDPM)

The RDPM concept used in this study corresponds to the one developed by Gerke and van Genuchten (1993). The model divides the flow domain into two overlapping and interacting continua according to the volumetric ratios of each domain, where two coupled 2-D Richards' equations are used to describe the matrix flow and preferential flow as

$$C_c(h)\frac{\partial h_c}{\partial t} = \nabla[K_c(h)\nabla(h_c+z)] - \frac{\Gamma_w}{w_c} \quad (5)$$

$$C_m(h)\frac{\partial h_m}{\partial t} = \nabla[K_m(h)\nabla(h_m+z)] + \frac{\Gamma_w}{w_m} \quad (6)$$

$$\Gamma_w = \alpha_w K_a(h_c - h_m) \quad (7)$$

$$w_c + w_m = 1 \quad (8)$$

$$\varepsilon = w_c\varepsilon_c + w_m\varepsilon_m \quad (9)$$

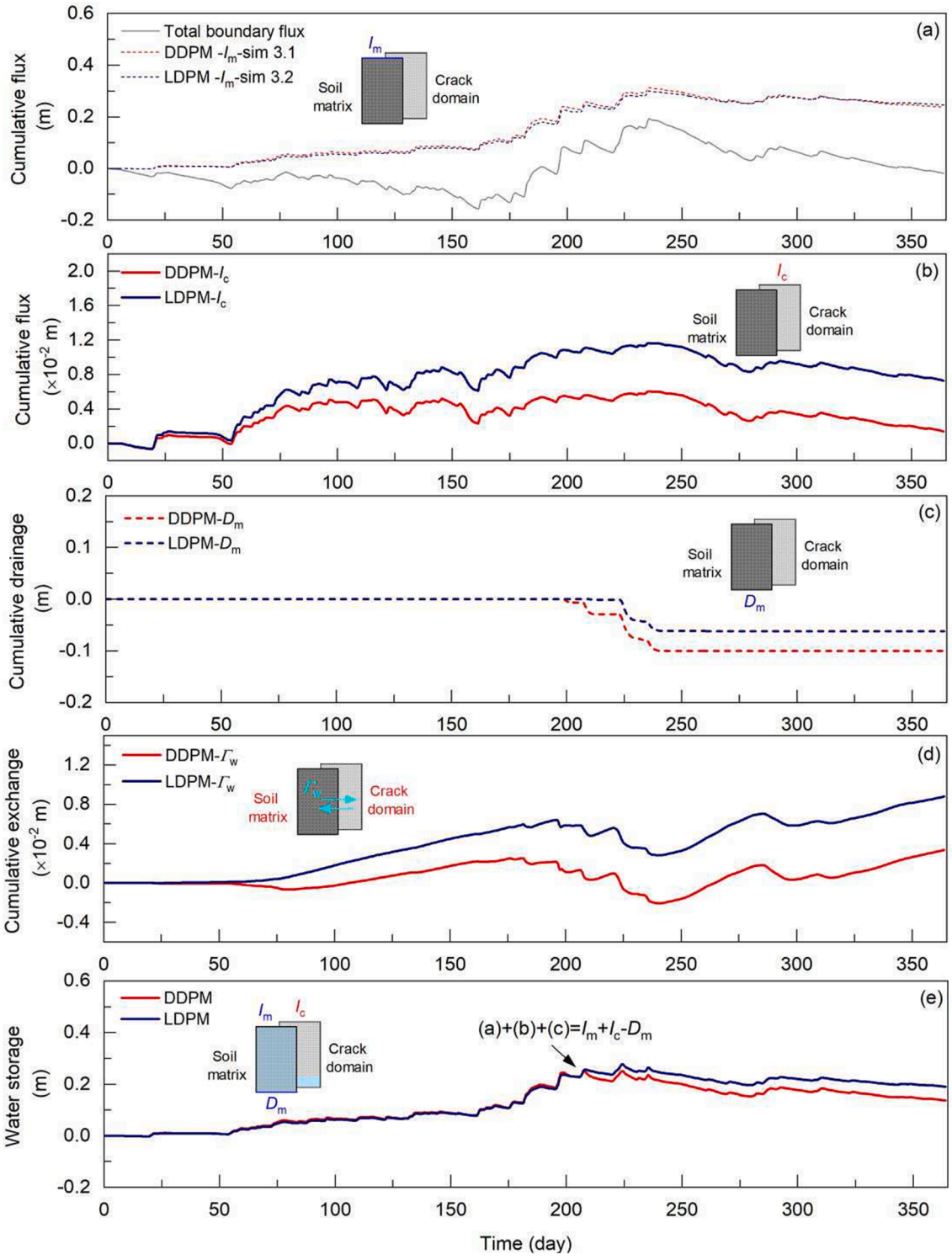

Fig. 10. Cumulative boundary water flux obtained from point B1 and B2 and corresponding water balance in the LDPM and DDPM. (a) cumulative matrix flux; (b) cumulative preferential flow flux; (c) cumulative drainage flux; (d) cumulative total water exchange; (f) temporal evolution of the water storage.

$$\theta = w_c\theta_c + w_m\theta_m \quad (10)$$

$$K = w_cK_c + w_mK_m \quad (11)$$

where

"c" and "m" indicate the crack and matrix domains, respectively;
h - the pressure head (m);
C - the specific water capacity, $d\theta/dh$ (1/m);
K - the isotropic hydraulic conductivity (m/s);
z - the elevation head (m);
w- the volumetric ratio of the crack domain or matrix domain over the bulk soil volume;
Γ_w- the water exchange term between the two domains (1/s);
α_w- the effective water transfer coefficient (1/m^2);
K_a - the interface hydraulic conductivity (m/s).

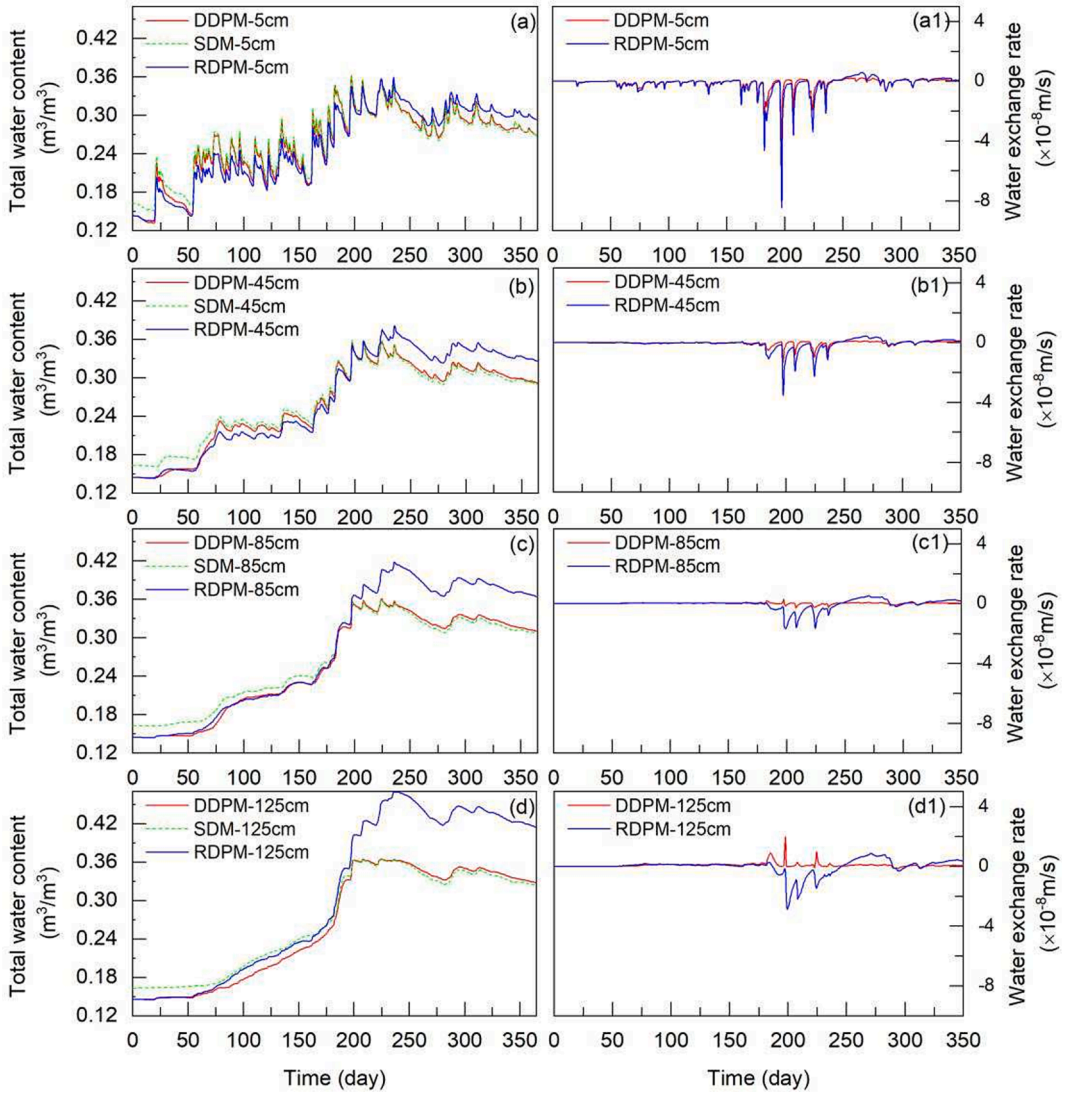

Fig. 11. Total water content and water exchange rate at monitoring point I1, I2, I3 and I4 in the DDPM, SDM and RDPM. (a) and (a1) 5-cm depth; (b) and (b1) 45-cm depth; (c) and (c1) 85-cm depth; (d) and (d1) 125-cm depth.

ε- the total pore volume divided by total soil volume. ε_m(or ε_c) is defined as the pore volume in matrix (or crack domain divided by the volume of that domain. The total volume water content, θ, has the same definition.

Regarding the α_w, it can be determined as follow

$$\alpha_w = \frac{\beta\gamma_w}{a^2} \tag{12}$$

where β is a dimensionless factor which depends on the shape of the soil matrix and is set as 3 following Aguilar-López et al. (2020), the γ_w is a dimensionless "scaling" coefficient with a suggested value of 0.4 (Gerke et al., 2007), and a is a scaling factor approximately equaling to the half width of the average block size.

As for the K_a, an improved K_a function reformulated by Gerke et al. (2013) is adopted.

$$K_{a_{\min}} = \begin{cases} \min\{K_m(h_c), K_c(h_c)\} & h_c \geqslant h_m \\ \min\{K_m(h_m), K_c(h_m)\} & h_c < h_m \end{cases} \tag{13}$$

This formulation represents that the flow occurs from the highest head toward the lowest head but regulated by the less permeable of the subsystems in that instant of time (Aguilar-López et al., 2020).

The hydraulic properties of the two domains are parameterized based on the Mualem-van Genuchten soil–water retention curves (SWRC) (Mualem, 1976; van Genuchten, 1980) as

$$S_e(h) = \frac{\theta - \theta_r}{\theta_s - \theta_r} = [1 + (|\alpha h|)^n]^{-m} \tag{14}$$

$$K_m(S_{e,m}) = K_{m,s}K_r(S_{e,m}) = K_{m,s}S_{e,m}^{0.5}\left[1 - \left(1 - S_{e,m}^{1/m_m}\right)^{m_m}\right]^2 \tag{15}$$

$$K_c(S_{e,c}) = K_{c,s}K_r(S_{e,c}) = K_{c,s}S_{e,c}^{0.5}[1 - (1 - S_{e,c}^{1/m_c})^{m_c}]^2 \tag{16}$$

where θ_s(-) and θ_r (-) are the saturated and residual volumetric water content, respectively; α(1/m), n(-) and l(-) are fitting parameters; K_r (-) is the relative hydraulic conductivity. Note that the $K_{m,s}$ and $K_{c,s}$ are fixed in the RDPM.

Different with the RDPM, we modified Eqs. (15) and (16) by combining Eqs. (2) and (4) to take the dynamic changes of the $K_{m,s}$ and $K_{c,s}$ into consideration (Luo et al., 2023). Meanwhile, we also set $K_r(S_{e,c})$ to 1 in Eq. (16). This modification ensures that the magnitude of K_c only depends on the crack aperture instead of the $S_{e,c}$, which can avoid the unreasonable low K_c at initial dry conditions or after long-term drying (Luo et al., 2023).

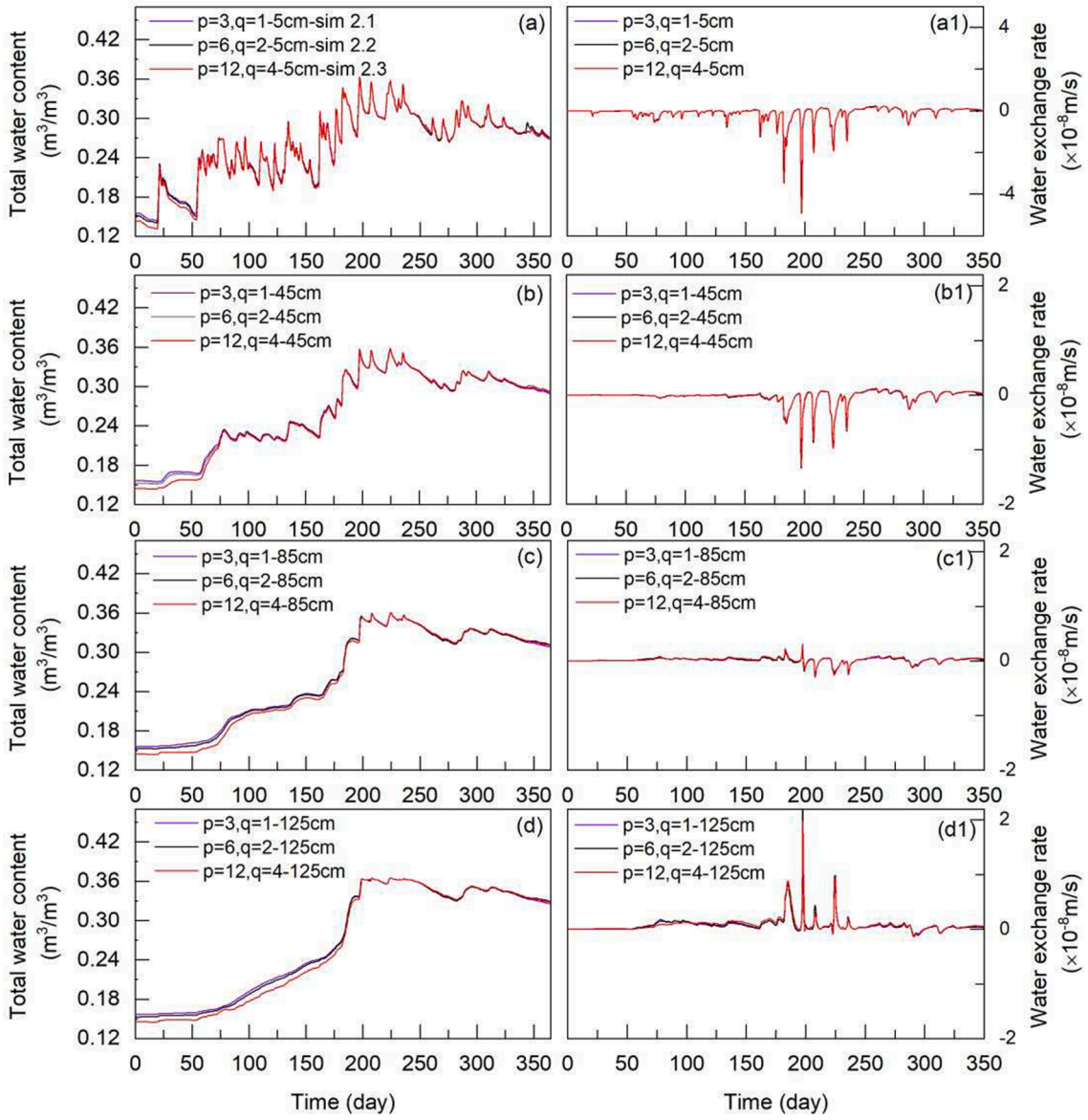

Fig. 12. Total water content and water exchange rate at monitoring point I1, I2, I3 and I4 in the sim 2.1, sim 2.2 and sim 2.3. (a) and (a1) 5-cm depth; (b) and (b1) 45-cm depth; (c) and (c1) 85-cm depth; (d) and (d1) 125-cm depth.

$$K_m(S_{e,m}) = K_{m,s}(S_{e,m})K_r(S_{e,m}) = K_{m,\max}\left(\frac{p+1}{p+S_{e,m}^{-q}}\right)S_{e,m}^{0.5}\left[1-\left(1-S_{e,m}^{1/m_m}\right)^{m_m}\right]^2 \quad (17)$$

$$K_c = K_{c,s}(S_{e,m}) = K_{c,\max}\left(\frac{1-S_{e,m}^{q}}{1+pS_{e,m}^{q}}\right)^2 + K_{c,\min} \quad (18)$$

In the case of a RDPM model, specified flux i is divided between the matrix and crack domains as

$$i = w_c i_c + w_m i_m \quad (19)$$

where i_c and i_m are the effective boundary fluxes into each domain (m/s).

Under rainfall conditions, the boundary transformation was achieved in COMSOL using a combined type of boundary (Dirichlet and Neumann) following Chui and Freyberg (2009) and Shao et al. (2015). Considering an evaporation condition, the Wilson-Fredlund-Barbour-Penman experimental function model Wilson et al. (1997) was used to calculate the actual evaporation of each domain (Luo et al., 2023).

3. Numerical experiments

3.1. Set-up of numerical model

The single-domain model (SDM), rigid dual-permeability model (RDPM) and dynamic DPM (DDPM) were implemented in a finite element solver for Richards equation as part of the COMSOL Multiphysics software (Comsol 5.6). As shown in Fig. 2, they have the same 2-D size, boundary conditions, mesh structure and initial condition. The model domain is 1.5 m high by 1.0 m wide. We are aware that desiccation cracks may extend to more than 1.5 m depth in some places (Bagnall et al., 2018; Neely et al., 2014; Neely et al., 2018), while the crack domain is still set as 1.5 m high as it is an average and representative value of desiccation cracks within atmosphere influence depth (0–3.0 m) in our experiences.

The left and right sides of the model were all no-flux boundaries; the top surface was set as a combined type of boundary conditions for representing the rainfall, ponding and evaporation process. For the matrix domain, the bottom side was a seepage boundary, while the bottom side for the crack domain was set as a no-flux boundary. The no-flux

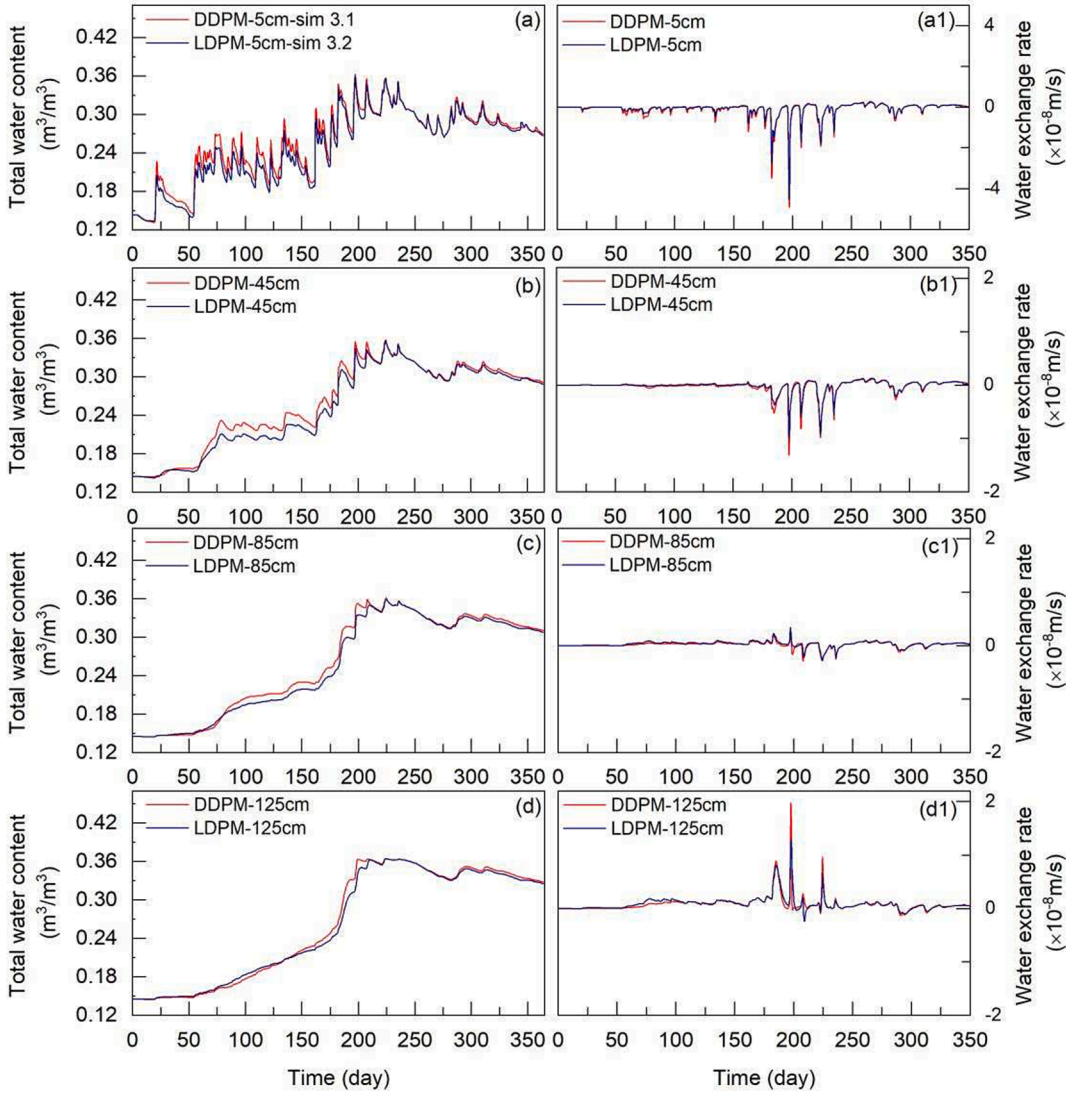

Fig. 13. Total water content and water exchange rate at monitoring point I1, I2, I3 and I4 in the LDPM and DDPM. (a) and (a1) 5-cm depth; (b) and (b1) 45-cm depth; (c) and (c1) 85-cm depth; (d) and (d1) 125-cm depth.

boundary of the crack domain was adopted mainly considering that in most shallow landslides induced by PF-DC, the desiccation cracks rarely cut through the overall soil layer or they penetrate the soil layer but are often limited by underlying low-permeability bedrock (Pei et al., 2020; Xie et al., 2020; Zhang et al., 2021a), and thus most of them are death-end macro pores (Greco, 2002).

Considering the PF-DC was common in our previous study areas, a typical region that is famous for widely-distributed cracked soils with different shrinking-swelling potential (Luo et al., 2021; Zhang et al., 2021a; Zhang et al., 2021b), one-year meteorological data (2021) from a weather station in Hefei, Anhui Province, China was used as the input of the top boundary. The time series of the meteorological data included daily rainfall r (mm/d), potential evaporation (PE mm/d), average temperature (T, ℃) and air relative humidity (RH, %), as shown in Fig. 3. We define June to August as the rainy season.

Because the pressure head in the surface area will change frequently during WD cycles, a mesh structure with dense boundary layers was used to capture the transient hydrological conditions. A coarser free-triangle mesh (average length of 0.1 m) was defined below the boundary layers. The initial pore water pressure (PWP) for all numerical models was set as −100 kPa. Two boundary monitoring points (B1 and B2) were set to record the infiltration flux and drainage flux. Four internal points at 5-cm (I1), 45-cm (I2), 85-cm (I3) and 125-cm (I4) depths were set to monitor the variation of the water content, water exchange rate and crack proportion.

3.2. Parameters

3.2.1. Shrinkage parameters

According to the empirical value provided by Stewart et al. (2016b) and our previous study (Luo et al., 2023), the four shrinkage parameters for the benchmark DDPM were set as $\phi_{\min} = 0.22$, $\phi_{\max} = 0.52$, $p = 12$, $q = 4$. As shown in Fig. 4, the variation of porosity in the matrix domain (ϕ_{matrix}) and the crack proportion (w_c) and can be obtained using Eqs. (1) and (3), respectively. Note that the minimum w_c calculated by Eq. (3) is set as 0.001 considering the incomplete closure of cracks during rainfall as observed in other studies (Coppola et al., 2012; Luo et al., 2021; Luo et al., 2023).

3.2.2. Soil water retention parameters

The soil water retention curves (SWRC) of each domain are presented in Fig. 5. Because the crack domain is a macropore-dominated space (Aguilar-López et al., 2020), the SWRC parameters of that domain were set with a greater saturated water content ($\theta_{c,s} = 0.99$), a lower value of

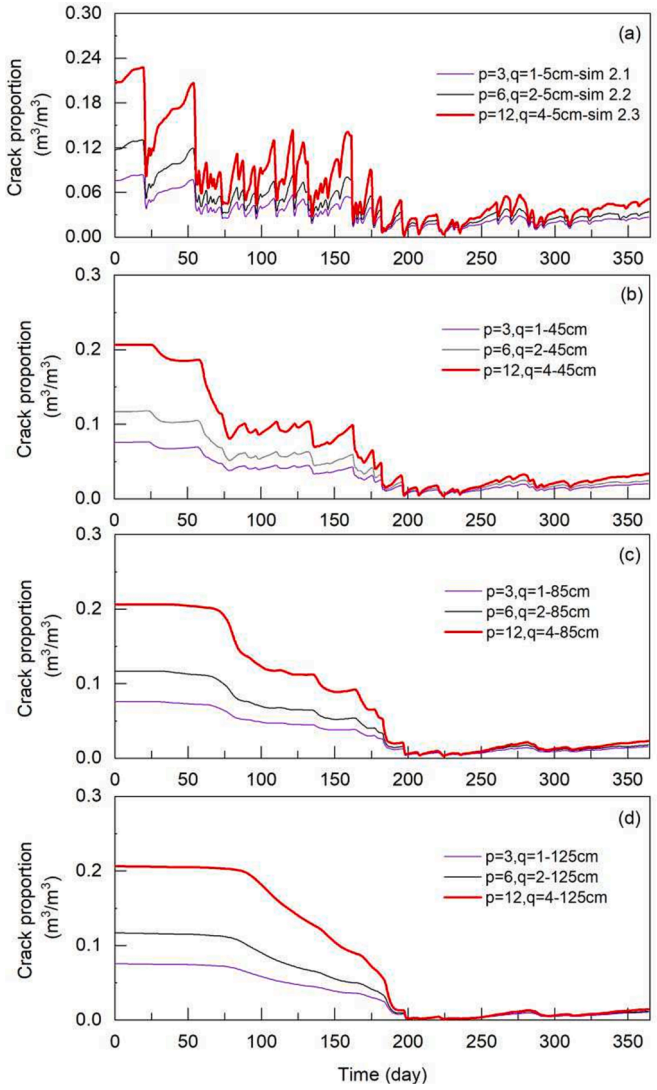

Fig. 14. Temporal evolution of crack proportion monitoring point I1, I2, I3 and I4 in the sim 2.1, sim 2.2 and sim 2.3. (a) 5-cm depth; (b) 45-cm depth; (c) 85-cm depth; (d) 125-cm depth.

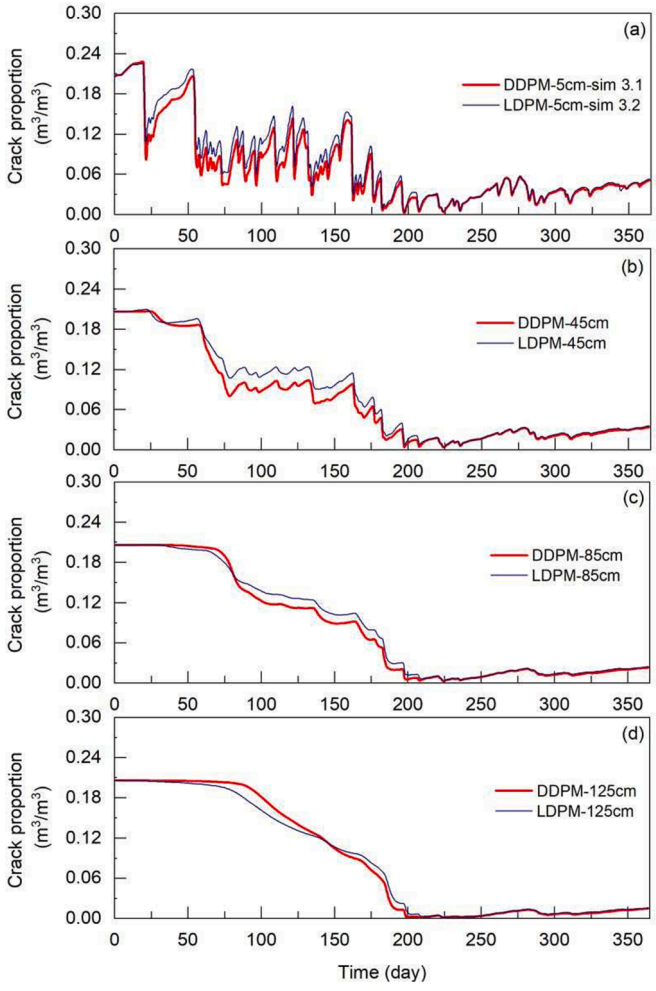

Fig. 15. Temporal evolution of crack proportion monitoring point I1, I2, I3 and I4 in the DDPM and LDPM. (a) 5-cm depth; (b) 45-cm depth; (c) 85-cm depth; (d) 125-cm depth.

air entry pressure (α_c=1.5) and a steeper slope (n_c = 2) than that of the matrix domain. All the SWRC parameters for each domain are fixed in the three models.

3.2.3. Hydraulic conductivity

The $K_{m,\max}$ is set to 5.55 × 10^{-7} m/s for representing low-permeable clay soils. Regarding the $K_{c,\max}$, it was calculated using Eq. (30) in Luo et al., 2023, where the $w_{j,\max}$ was set to 2.6 mm. Then, the variation curve of transient saturated hydraulic conductivity of the matrix domain ($K_{m,s}$) and the crack domain ($K_{c,s}$) can be obtained using Eqs. (2) and (4), respectively. The $K_{c,\min}$ was also estimated using Eq. (30) in Luo et al (2022) with a suggested $w_{j,\min}$ value of 0.01 mm. Further, the variation of K_m and K_c with the pressure head (h) in the DDPM can be calculated by combining Eqs. (17) and (18). Fig. 6 shows the variation curves of K_m and K_c. Regarding the water transfer coefficient α_w, it is set as 120 1/m^2 according to Eq. (12) by assuming the half width of the average soil matrix equals to 100 mm (see Fig. 1).

3.3. Experiments

3.3.1. Experiment 1: Dynamic changes of crack volume and hydraulic properties

This experiment is conducted to compare the performance of SDM, RDPM and DDPM under WD cycles. For comparison, the SWRC parameters and hydraulic properties of soil in the SDM are set as the same as that of the matrix domain in the RDPM. The crack proportion (w_c) used in the RDPM equals to the initial crack proportion obtained in the DDPM (w_c = 0.206).

3.3.2. Experiment 2: Shrinking-swelling parameters p and q

The shrinking-swelling ability of soils acts not only on the proportion shift of the two domains during wetting and drying, but also on the variation of hydraulic properties of each domain. This experiment aims on testing the sensitivity of the DDPM to the shrinking-swelling parameters by altering p and q while fixing $\phi_{\max}$ and $\phi_{\min}$. Fig. 7 shows the shrinking-welling curves with different p and q and corresponding hydraulic conductivity of each domain. The soil with (p = 12, q = 4) has the highest shrinking-swelling ability, followed by (p = 6, q = 2) and (p = 3, q = 1). Note that the aforementioned three suites of shrinking-swelling parameters were select because they have universal representativity for the cracked soils with shrinking-swelling ability from high to low. Additionally, the hysteresis effects during WD cycles are not considered.

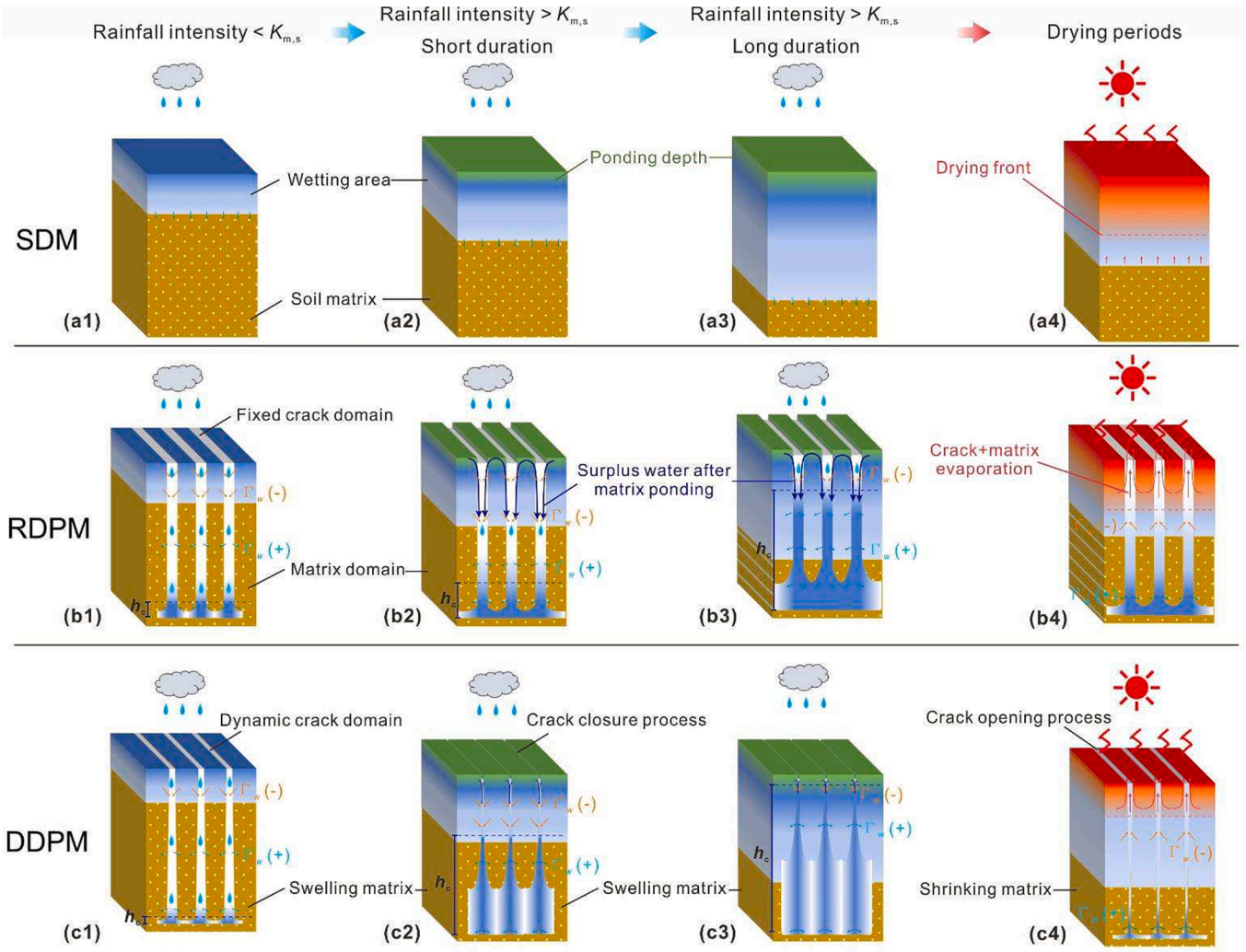

Fig. 16. Diagram of water infiltration and evaporation in different models. (a1–a4) Water infiltration and evaporation simulated by SDM; (b1–b4) Water infiltration and evaporation simulated by RDPM; (c1–c4) Water infiltration and evaporation simulated by DDPM. $\Gamma_w(+)$ refers to water transfers from the crack domain to the matrix domain, while $\Gamma_w(-)$ refers to the opposite direction.

3.3.3. Experiment 3: Fixing hydraulic properties while only changing crack proportion

Building on the classical DPM concept, a simple way to simulate PF-DC, which incorporates an empirical function of crack proportion *vs* water content into the RDPM but neglects the changes of hydraulic properties in each domain, is easy to figure out and applied (Lepore et al., 2009; Luo et al., 2021). To test the rationality of such a "lighter" dynamic DPM (LDPM), we only incorporate Eq. (3) to the RDPM while fixing other parameters to see the difference between the LDPM and DDPM.

A summary of the fixed and varied parameters in each experiment are presented in Tables 1 and 2, respectively.

4. Results

4.1. Boundary water flux and water balance

Figs. 8–10 show the hydrological results including integrated upper boundary flux, drainage, water exchange and water storage for the three experiments. The corresponding transient hydrological results can be found in Appendix. Note that the positive value of the water exchange refers to water moving from the crack domain to the matrix domain, while negative for the opposite direction. The cumulative flux of each domain in the dual-permeability models (DDPM, RDPM and LDPM) is actual value that has been multiplied by their respective proportions (see Eq. (19)). Besides, in all the graphs involving the integrated flux and water storage, the steep increase stage of each curve represents cumulative infiltration water flux during wetting periods, while the gradual decrease stage represents cumulative outflow water flux during drying and drainage periods.

4.1.1. Experiment 1

As shown in Fig. 8a, the matrix flow dominates the soil infiltration process in the DDPM, where the preferential flow only accounts for approximately 2%-8% of the total inflow flux. For the RDPM, the matrix flow in the RDPM is 6%-25% less than that of the SDM and DDPM, but its preferential flow through the fixed crack paths is 68%-98% larger than that of the DDPM. Overall, the total infiltration of the RDPM is 10% and 12% larger than that of the SDM and DDPM, respectively.

For the evaporation periods, the matrix domain in the dual-permeability models still dominates the evaporation process, where matrix evaporation in the DDPM accounts for approximately 91% of the total evaporation, while the matrix evaporation in the RDPM accounts for 80% of the total evaporation. Note that at approximately the first 50 days, the DDPM simulated larger crack evaporation than that of the RDPM. After that, the crack evaporation simulated by the RDPM is on average 30% higher than that of the DDPM. Interestingly, the total evaporation simulated by the three models is close to each other, with a

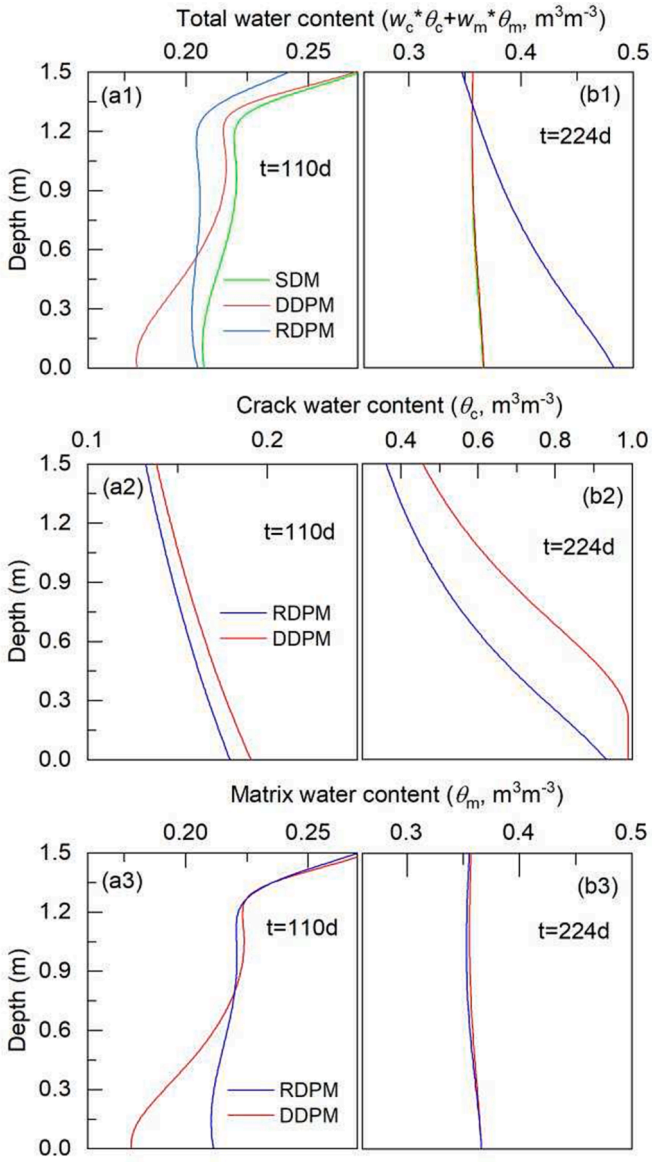

Fig. 17. Vertical distribution of total water content and effective water content in each domain simulated by different models. (a1), (a2) and (a3) represent total water content, crack water content and matrix water content before the rainy season; (b1), (b2) and (b3) represent total water content, crack water content and matrix water content during the rainy season.

maximum difference of 3%.

In Fig. 8b, c, the water drainage in all three models appeared in August and September following four significant rainfall events. The cumulative drainage simulated by the SDM is the largest, which is 15% and 60% higher than that of the DDPM and RDPM, respectively. It seems to be abnormal that the RDPM with the maximum fixed crack proportion has the minimum drainage capacity. However, if we recall that the bottom boundary of the crack domain is a no-flux boundary and look at Fig. 8c, it can be found that the water mainly exchanges from the matrix to the crack domain in the RDPM (more negative value), while the DDPM shows the opposite result. It indicates that most of the water in the RDPM has been stored in the crack domain instead of being drained from the matrix domain during rainfall seasons. Consequently, the cumulative water storage in the RDPM is the largest (Fig. 8d). Additionally, the desiccation cracks in the DDPM also have more water storage space with respect to the SDM, and therefore its cumulative water storage is slightly higher than the SDM.

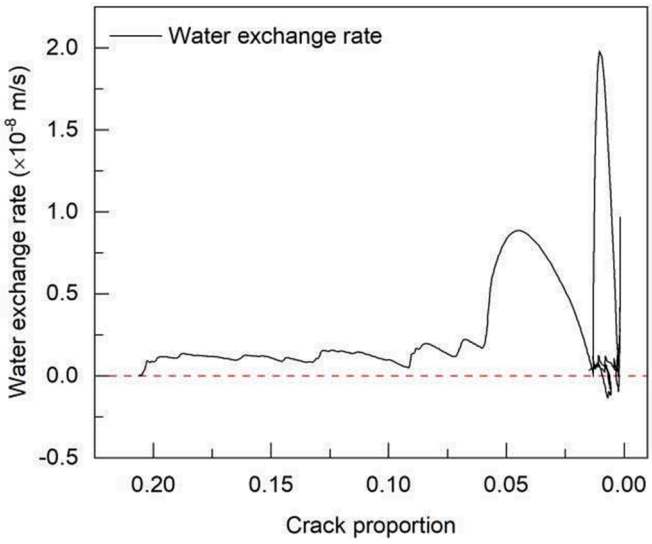

Fig. 18. Crack proportion versus water exchange rate at 125 cm depth in DDPM. Note that as the rainfall intensity fluctuates in our study, the curve shows a nonmonotonic increasing trend.

4.1.2. *Experiment 2*

In this section, we first recall that the sim 2.1, sim 2.2 and sim 2.3 represent soils with weak, moderate and high shrinking-swelling ability, respectively, and their shrinking-swelling ability increases progressively by two times. As shown in Fig. 9a, the cumulative matrix flux decreases by approximately 1.02 times with the increase of soil shrinking-swelling ability. But for the crack domain (Fig. 9b), the cumulative preferential flow and crack evaporation of the sim 2.3 is (27%, 43%) and (36%, 54%) larger than that of sim 2.2 and sim 2.1, respectively. This result indicates that the soil shrinking-swelling ability has a greater influence on the crack domain than the matrix domain. For the drainage process (Fig. 9c), it is negatively correlated with the shrinking-swelling ability. The sim 2.1 has the highest drainage and its cumulative drainage is 5% and 15% larger than the sim 2.2 and sim 2.3, respectively. In Fig. 9d, the three simulations show a similar trend of water exchange. It demonstrates that the higher soil shrinking-welling ability has lower positive water exchange before the rainy season, but it comes to the opposite result after the rainy season. With regard to water storage, it is negatively correlated to the shrinking-swelling ability prior to the rainy season but is positively correlated to the shrinking-swelling ability after the rainy season. The ultimate water storage in the sim 2.3 is 6.2 mm and 12.7 mm larger with respect to sim 2.2 and sim 2.1, respectively. Overall, the differences in the concerned hydrological results among the three simulations are not as significant as that in *experiment 1*.

4.1.3. *Experiment 3*

As shown in Fig. 10a, prior to October, the matrix infiltration and evaporation simulated by the DDPM are overall higher than that of the LDPM, but the ultimate cumulative matrix flux in the DDPM is 9.1 mm lower with respect to the LDPM.

For the crack domain (Fig. 10b), the crack evaporation rate in the DDPM is slightly higher than that of the LDPM but its preferential flow rate is much smaller with respect to the LDPM. Hence, the ultimate cumulative preferential flow flux in the DDPM is 5.8 mm lower than that of the LDPM. During the drainage process (Fig. 10c), the DDPM shows earlier drainage and overall higher drainage rate than that of the LDPM and its ultimate cumulative drainage is 38.7 mm larger with respect to the LDPM. In Fig. 10d, the DDPM and LDPM have a similar water exchange trend, but the LDPM has higher positive water exchange rates and its ultimate cumulative water exchange is 5.4 mm. With regard to water storage, the DDPM is slightly higher than that of the LDPM prior to

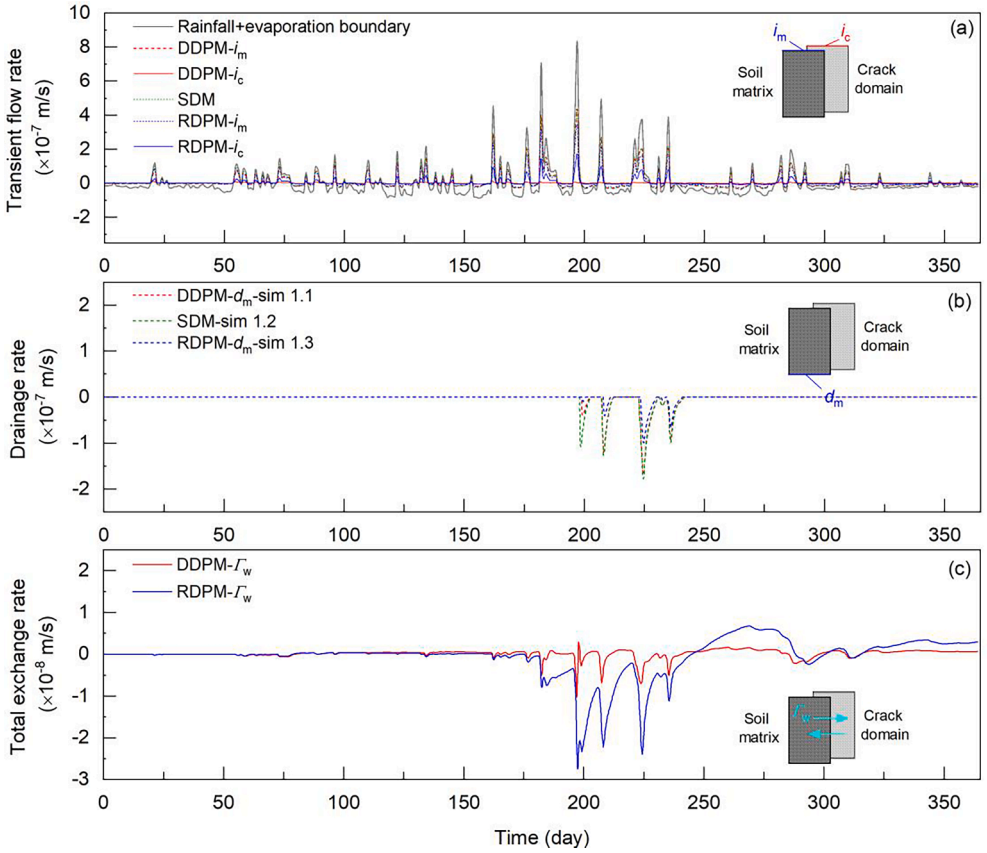

Fig. A1. Transient boundary water flux obtained from point B1 and B2 and corresponding water balance of the DDPM, SDM and RDPM. (a) the transient boundary flow rate of the three models; (b) the transient drainage rate; (c) the total water exchange rate of the DDPM and RDPM.

the rainy season but it comes to the opposite result since the rainy season. The ultimate water storage simulated by the DDPM is 53.8 mm lower than the LDPM, which can mainly be ascribed to the more drainage in the DDPM.

4.2. Water content

Figs. 11–13 show the total water content and water exchange rate at monitoring point I1, I2, I3 and I4 in the three experiments. The graphs on the left are results of the total water content while the graphs on the right are results of water exchange rate. Note that the total water content in the DDPM, RDPM and LDPM is calculated by Eq. (10).

4.2.1. Experiment 1

As shown in Fig. 11, before the rainy season, the water content at all depths simulated by the SDM is higher with respect to the DDPM and RDPM, but it becomes the lowest after the rainy season. Additionally, from nearly the 25th to the 50th day, it can be found that both the DDPM and RDPM simulated an earlier increase of water content in deep soil (85–125 cm) with respect to the SDM. This kind of 'non-sequential' hydrological response induced by preferential flow has been widely observed in some field and laboratory experiments (Lin and Zhou, 2007; Luo et al., 2021; Zhang et al., 2021a). Regarding the DDPM and RDPM, prior to the rainy season, the DDPM shows overall higher water content than that of the RDPM at shallow depths (i.e. 5–45 cm), but the water content simulated by the DDPM gradually becomes smaller than that of the RDPM with the increase of soil depths. After the rainy season, water content simulated by the RDPM at all depths is higher than that of the DDPM and their differences become larger with the increase of soil depths.

Further looking at the water exchange rate, the negative water exchange (from the matrix to the crack domain) dominates the shallow soil depths (i.e. 5–45 cm) in both the DDPM and RDPM, where the significant peak negative water exchange rates appeared mainly during the rainy season. However, the negative water exchange gradually becomes smaller with the soil depths. Particularly, the water exchange rates in the deep soils (i.e. 125 cm) simulated by the DDPM almost all change to positive values while the RDPM still has significant negative water exchange rates. Nevertheless, following the rainy season, the RDPM shows higher positive water exchange rates than that of the DDPM.

4.2.2. Experiment 2

As shown in Fig. 12, the differences in water content among sim 2.1, sim 2.2 and sim 2.3 mainly appear in deep soil depths (85–125 cm) prior to the rainy season. Their differences are shown as the water content decreases with the increase of soil shrinking-swelling ability. However, the differences at all depths become insignificant following the rainy season. For the water exchange rates, their differences at all depths among the three simulations are insignificant.

4.2.3. Experiment 3

As shown in Fig. 13, the DDPM shows overall higher water contents with respect to the LDPM at all depths, where the differences prior to the rainy season are more significant than those after the rainy season. But the differences become smaller with the soil depths. At different depths from top to bottom, the average water content simulated by the DDPM is 0.8%, 0.75%, 0.5% and 0.2 % higher than that of the LDPM. For the water exchange rates, the LDPM has a similar trend with the DDPM, where the DDPM shows higher negative water exchange rates in shallow soil depths (5–45 cm) while it shows higher peak positive water exchange rates during the rainy season at 125-cm depth. Overall, the

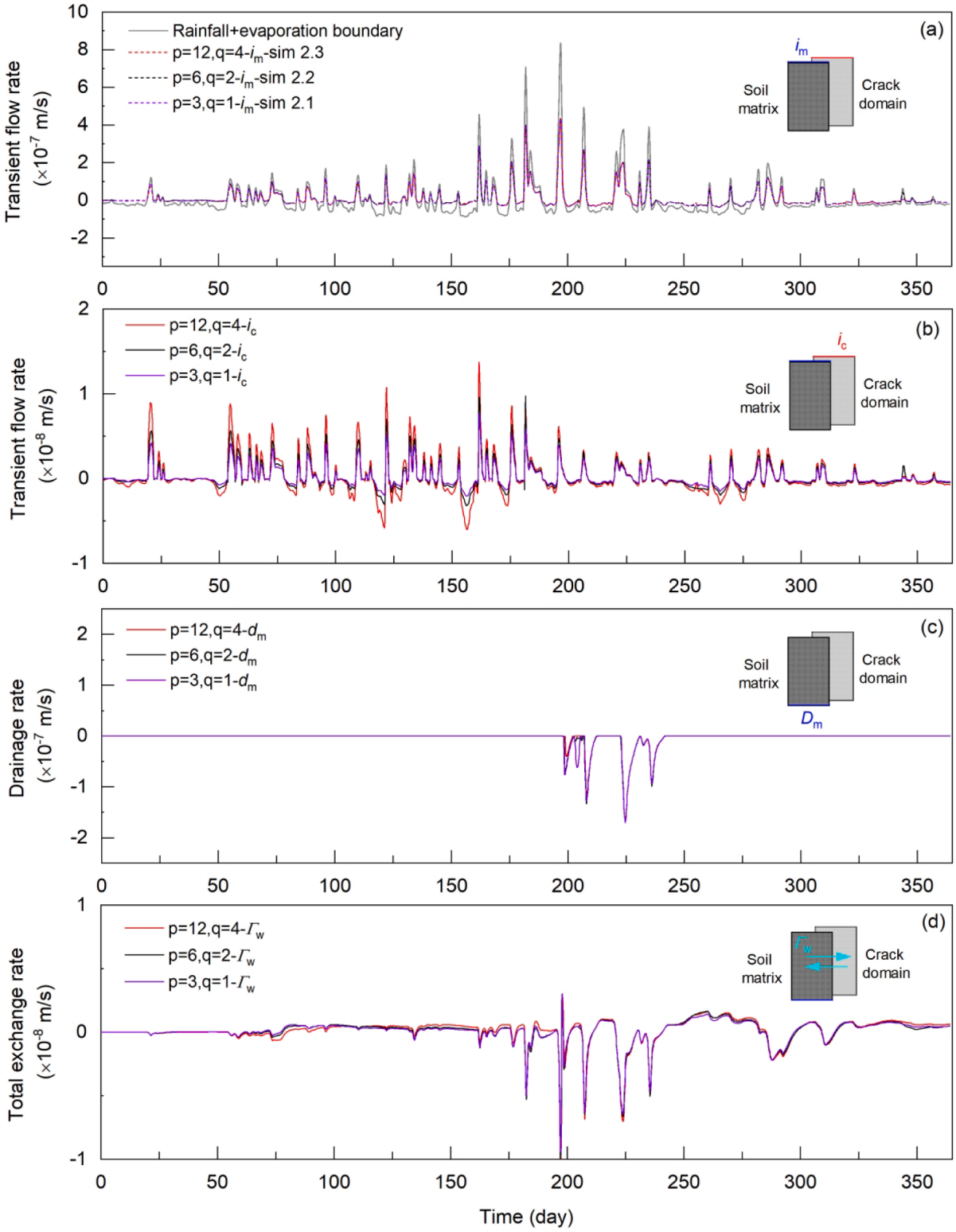

Fig. A2. Transient boundary water flux obtained from point B1 and B2 and corresponding water balance in the sim 2.1, sim 2.2 and sim 2.3. (a) transient matrix flow rate; (b) transient preferential flow rate; (c) transient drainage rate; (d) total water exchange rate.

LDPM at all depths simulated lower negative and slightly higher positive water exchange rates with respect to the DDPM.

4.3. Crack proportion

Figs. 14 and 15 show the temporal evolution of crack proportion at different depths in *experiment 2* and *experiment 3*. The crack proportion is calculated using Eq. (3).

4.3.1. Experiment 2

As shown in Fig. 14, the crack proportion in shallow soil depths shows more sensitivity to the boundary alteration. It increases during

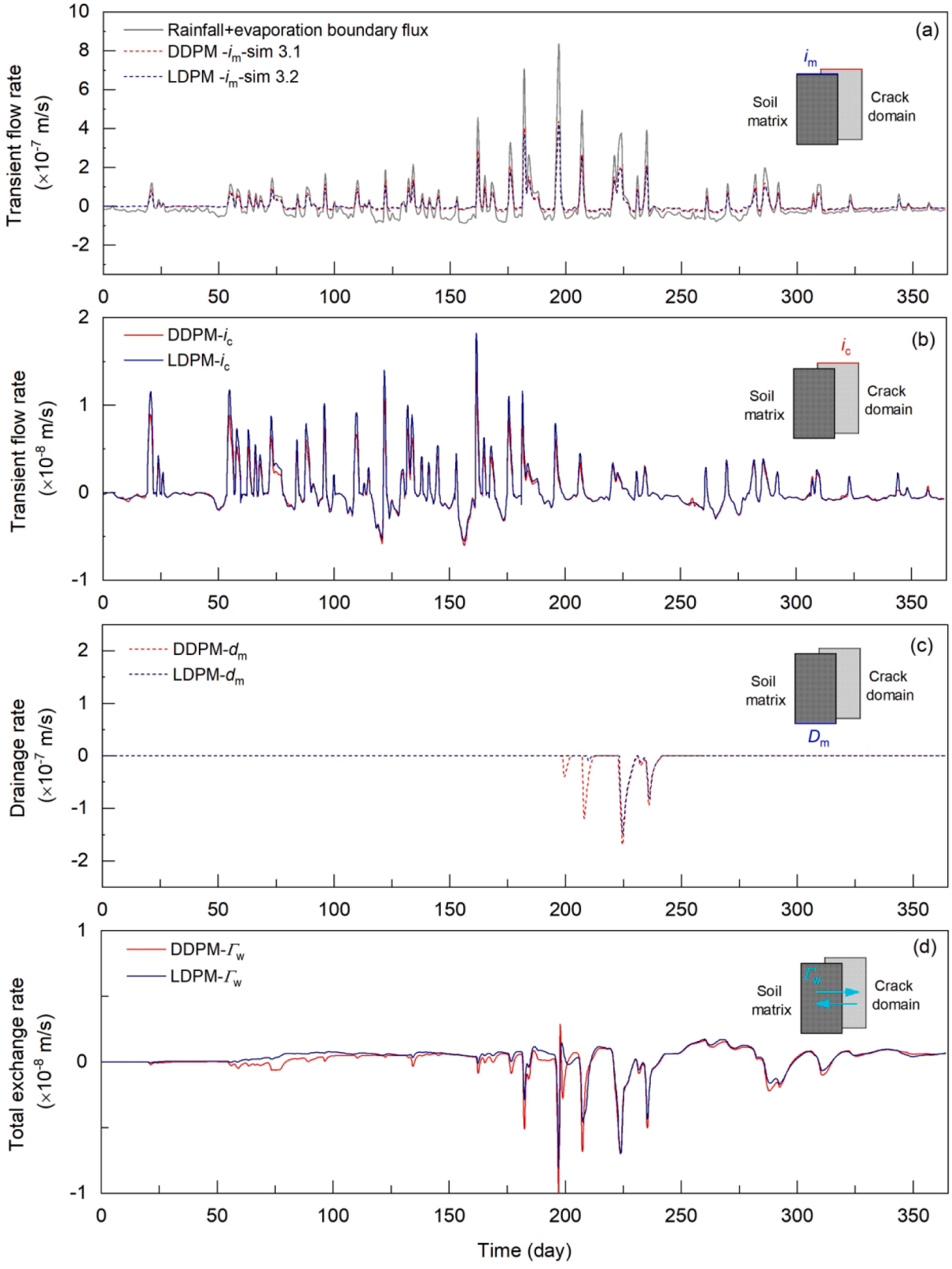

Fig. A3. Transient boundary water flux obtained from point B1 and B2 and corresponding water balance in the LDPM and DDPM. (a) transient matrix flow rate; (b) transient preferential flow rate; (c) transient drainage rate; (d) total water exchange rate.

drying periods and decreases during wetting periods. However, the crack proportion in deep soils (i.e. 85–125 cm) shows basically decline trend with much less fluctuations. Overall, the crack proportion has an overall positive correlation with the soil shrinking-swelling ability. Additionally, it can be found that prior to the rainy season, the crack proportion in the sim 2.3 is approximately 2 and 3 times higher than that in the sim 2.1 and sim 2.2, respectively. However, their differences become much smaller after the rainy season, and the crack proportion in the three simulations almost overlaps with each other at the 125-cm depth.

Experiment 3: In Fig. 15, the crack proportion simulated by the LDPM is overall larger with respect to the DDPM. The differences between the LDPM and DDPM mainly appear before the rainy season and their differences become smaller with the soil depths. An interesting phenomenon is that the crack proportion in the DDPM gradually becomes larger than that of the LDPM with the increase of soil depths. For the crack proportion after the rainy season, the LDPM and DDPM almost overlaps with each other at all depths.

5. Discussions and conclusions

5.1. Water flow and distribution in different models

Fig. 16 shows the conceptual diagram of water infiltration and evaporation in the SDM, RDPM and DDPM models. Prior to the discussions, we must point out that in some cases, the desiccation cracks may be deeper than the 1.5 m boundary condition assumed in this work (Bagnall et al., 2019; Bagnall et al., 2018; Baram et al., 2013; Neely et al., 2014). In such cases, cracks may cut through the soil layer and connect to the groundwater, which will lead a large part of water to discharge into the groundwater. In these cases, our current boundary setting of the crack bottom will lose its universal significance. Indeed, such a condition is another interesting, complex and widely concerned issue worthy of in-depth discussion but is beyond the scope of this current work depicted in Fig. 16.

(i) Low rainfall intensity (e.g. periods prior to the rainy season in this study).

When the rainfall intensity is lower than the matrix infiltrability (Fig. 16a1, b1 and c1), no overland flow will appear on the matrix domain and the preferential flow rate in the desiccation cracks equals to that of the matrix. All rainfall infiltrates into the soil in the SDM, RDPM and DDPM. It means that the preferential paths prior to the rainy season have little contribution to the overall soil infiltration flux. Note that because the surficial cracks in the DDPM diminish with the surrounding matrix becoming wetting, the weighted preferential flow flux (w_c*i_c) in that model is lower with respect to the RDPM but the weighted matrix flow flux (w_m*i_m) of the DDPM is higher than that of the RDPM. In any case, under low rainfall intensity, the summation of boundary infiltration flux in the crack and matrix domains simulated by the RDPM and DDPM equals to that of the SDM. However, the moisture distribution in the three models differs much from each other.

Fig. 17 shows the vertical distribution of simulated total water content and effective water content in each domain before and during the rainy season. Firstly, let us recall Eq. (10) and it can be inferred that when the water content of the crack domain is higher than that of the soil matrix, the cracks will always lead to a higher total water content than that without cracks. Then, keep it in mind and look at Fig. 16b1 and c1, the crack domain both in the RDPM and DDPM remains overall unsaturated because most water infiltrating into that domain has rapidly transferred to the surrounding soil matrix. Such a result leads to the crack domain maintaining a relatively drier condition than the surrounding matrix (Fig. 17a2-a3). Hence, the total water content in all depths modeled by the RDPM and DDPM is smaller with respect to the SDM (Fig. 17a1). Additionally, due to the diminishing proportion of the dry crack domain in shallow depths, the total water content in the DDPM is higher with respect to the RDPM. Conversely, in the deep soils, the bottom crack domain both in the RDPM and DDPM is moister than in shallow depths. In this case, the diminishing crack proportion in the DDPM plays a negative role in raising the total water content. Consequently, the total water content in deep soils simulated by the DDPM is below that of the RDPM. Notably, the response time of the water content of the deep soils in the two dual-permeability models is earlier with respect to the SDM because of the preferential flow.

Regarding the water exchange rate, because the matrix domain at shallow depths gets saturated earlier than the crack domain, the negative water exchange rate dominates the shallow water transfer process. It is precisely because of this part of supplementary water coming from the shallow soil matrix, the bottom crack domain during low rainfall intensity formed a moister zone than shallow depths. For the same reason, this part of water promotes the water exchange from the crack domain into the matrix domain in deep soils. However, the cumulative water exchange into the deep soil matrix is not enough to saturate that domain, and therefore no water drainage appeared during the periods before the rainy season. Remember that water will not drain through the crack domain because its bottom boundary was set as a no-flux boundary.

(ii) Heavy rainfall intensity (e.g. during the rainy season).

As shown in Fig. 16a2-c2 and a3-c3, the heavy rainfall intensity leads to water ponding on the matrix surface. The surplus water in the SDM is lost as surface runoff while that in the RDPM and DDPM flows into the crack domain as preferential flow. When the heavy rainfall lasts short duration, the cumulative preferential flow fluxes can only wet a small part of the fixed crack domain in the RDPM (Fig. 16b2). Conversely, due to the diminishing crack volume in the DDPM, the same cumulative preferential flow fluxes in the RDPM will lead to a higher wetting zone in the crack domain of the DDPM (Fig. 17b2). By interrelating the crack proportion with the water exchange rate under rainfall (Fig. 18, take 125 cm depth as an example), it is found that the positive water exchange rates overall increased with the decrease of crack proportion. We infer that the crack closure process benefits the building-up of pore water pressure in the crack domain and therefore promotes water exchanges from the crack to the matrix domain. Consequently, in most depth ranges, the positive water exchange rates appear earlier in the DDPM with respect to the RDPM (Fig. 11a1–d1). However, when it comes to the long-duration heavy rainfall (Fig. 16b3 and c3), the large amount of water will saturate the crack domain both in the RDPM and DDPM (not in our current modeling). Their water exchange rates all become positive value when the surrounding soil matrix is at unsaturated state. In our study, due to the crack closure effect, the water content in the crack domain modeled by the RDPM are overall lower with respect to the DDPM (Fig. 17b2), but its fixed crack proportion is much larger than the reduced crack proportion in the DDPM. Therefore, the RDPM shows significantly higher total water content with respect to the DDPM. For the same reason, the DDPM has an over moister crack domain than its matrix domain (Fig. 17b2-b3), and therefore its total water content is slightly higher than the SDM (Fig. 17b1). Their differences mainly depend on the minimum crack proportion in Eq. (3).

(iii) Evaporation process

As shown in Fig. 16a4–c4, the drying front depth of the soil matrix in the RDPM and SDM is similar to each other while that in the DDPM is shallower than other two models. It can be ascribed to the permeability decay effects induced by matrix shrinkage during drying (see Eq. (17), Fig. 6a), which leads to the effective matrix evaporation rate of the DDPM is overall smaller with respect to the SDM and RDPM. However, when comparing the weighted matrix evaporation rate (w_m*i_m) in this study, the RDPM becomes smaller than that of the DDPM because of its

low matrix proportion ($w_m = 0.794$). Regarding to the crack domain, it can promote the overall soil evaporation by leading water exchange from the soil matrix to the crack domain, but the RDPM and DDPM have different performance. For the DDPM, the matrix evaporation during drying enlarges the desiccation cracks and thus increases the hydraulic conductivity of the crack domain (see Eq. (18) and Fig. 6b). This result means that under long-term drought, the drying front in the DDPM can keep moving deeper along the desiccation cracks once the water content of the surrounding soil matrix is still higher the residual water content. However, for the RDPM, once the water content of the crack domain equals to the residual water content (or the crack domain is empty), the hydraulic conductivity of the crack domain will decrease to nearly zero with the drying process proceeding (Eq. (16), Fig. 6b). Hence, under long-term drought, the RDPM will greatly underestimate the evaporation from the crack domain. In our current study, the crack domain in most periods is at relatively moist state due to insufficient drought. It means the crack evaporation mainly depends on the surficial crack proportion. Consequently, the crack evaporation modeled by the RDPM after the 50th day is higher than that of the DDPM.

5.2. Implications of the numerical experiments

In this study, because the DDPM has been validated in our recent work (Luo et al., 2023), we tentatively acquiesce the DDPM ($p = 12$, $q = 4$) as a benchmark model. As a result, the deviations between other models and DDPM are regarded as prediction errors. Building on the simulation results and analysis above, it can be found that the SDM overestimated the water content during low-intensity rainfall periods while underestimating the water content during heavy rainfall periods. Meanwhile, the SDM failed to simulate the 'no-sequential' hydrological response induced by the preferential flow. This may be detrimental to using the SDM to evaluate the migration of water pollution or the water content threshold of a landslide. For the RDPM, it greatly overestimated the total water content and the water storage capacity of the crack domain, which could be extremely dangerous to be used in surface runoff or floods forecast. For instance, the recent study conducted by Morales et al. (2021) showed that the desiccation cracks have limited contribution to intercepting the flood water. For the LDPM, it underestimates the total water content while overestimating the contribution of preferential flow to the soil matrix, which may overestimate the irrigation efficiency in the cracked farmlands. Additionally, the LDPM overestimates the overall water storage capacity of the soil and thus is also improper to be used to predict surface runoff and floods. However, the deviations caused by the LDPM are still smaller compared to the RDPM. Most importantly, the LDPM shows the most approaching results of the water content and crack evolution to that of the DDPM. Consequently, we suggest that when the specific shrinking-swelling parameters of soils are absent while the empirical relationships between the crack proportion and soil water content can be measured (Luo et al., 2021), the LDPM can be a tentative alternative option for the DDPM in simulating landslide hydrology, but it is better not to use it to evaluate the solutes transport and surface runoff or use it under long-term extreme drought.

Another important result in this study is that during heavy rainfall periods, the hydrological results simulated by the DDPM are not sensitive to the soil shrinking-swelling ability. Indeed, it is reasonable in practice. As we mentioned in section 3.3, the shrinking-swelling ability of soils mainly has two aspects of influence on the soil: the proportion shift and the variation of hydraulic properties of the two domains. From the hydrological-driven perspective, the dynamic changes of the desiccation cracks are directly dominated by the water content of the soil matrix. The water content of the soil matrix at any depth mainly depends on hydraulic conductivity. Looking back at Fig. 7b, under relatively moist soil conditions (PWP ranges from −10 kPa to 0 kPa), the differences in matrix hydraulic conductivity among the soils with different shrinking-swelling abilities are within one order of magnitude. This means that under heavy rainfall, the surface soil matrix will rapidly get saturation and the desiccation cracks in soils with different shrinking-swelling abilities all quickly diminish to the minimum crack proportion. Consequently, the differences in the crack proportion at different water content among the soils with different shrinking-swelling abilities will be reduced (see Fig. 13). Interestingly, Bagnall (2014) obtained similar results.

In conclusion, the prediction errors without considering crack evolution and variation of hydraulic properties (RDPM) are the highest, then followed by the only considering crack evolution (LDPM) and uncertainties of shrinking-swelling parameters. The single-domain model neglecting cracks and rigid dual-permeability model neglecting dynamic changes of desiccation cracks are all not recommended to simulate PF-DC. A lighter dynamic dual-permeability model only considering crack evolution can tentatively substitute the full dynamic dual-permeability model in specific cases.

6. Funds

This work was financially supported by the National Natural Science Foundation of China (42177166) and the Fundamental Research Funds for National University, China University of Geosciences (Wuhan). It was also partially funded by the Plan of Anhui Province Transport Technology Progress (grant 2018030) and Engineering Research Center of Rock-Soil Drilling & Excavation and Protection, Ministry of Education (202210).

Declaration of Competing Interest

The authors declare that they have no known competing financial interests or personal relationships that could have appeared to influence the work reported in this paper.

Data availability

Data will be made available on request.

Acknowledgments

This paper was written during visiting research exchange of Yi Luo at TUDelft in Summer 2022. Professor Thom Bogaard, Aguilar-López, Juan P and Roberto Greco are thanked for discussion and comments to our model and an earlier version of this paper which greatly helped structuring this manuscript. The authors also would like to thank the editor and anonymous reviewers for their valuable comments that substantially improved this paper.

Appendix A

Figs. A1–A3 show the hydrological results including transient upper boundary flux, drainage, water exchange and water storage for the three experiments. Note that the positive value of the water exchange refers to water moving from the crack domain to the matrix domain, while negative for the opposite direction. The flow rate of each domain in the dual-permeability models (DDPM, RDPM and LDPM) is the actual value that has been multiplied by their respective proportions (see Eq. (19)). The transient hydrological results are presented here for the sake of showing the numerical stability of the models based on the COMSOL Multiphysics.

References

Aguilar-López, J.P., Bogaard, T.A., Gerke, H.H., 2020. Dual-permeability model improvements for representation of preferential flow in fractured clays. Water Resour. Res. 56 https://doi.org/10.1029/2020wr027304.

Bagnall, D.K., 2014. Testing a mesopore and matrix model for use on shrink–swell soils. Texas A&M Univ, College Station, TX. M.S. thesis.

Bagnall, D.K., Crespo Gutierrez, P.M., Yimam, Y.T., Morgan, C.L.S., Neely, H.L., Ackerson, J.P., 2018. Effect of air- and water-filled voids on neutron moisture meter measurements of clay soil. Vadose Zone J. 17, 1–9. https://doi.org/10.2136/vzj2018.07.0137.

Bagnall, D., Morgan, C.L.S., Molling, C.C., Heilman, J.L., Moore, G.W., 2019. Testing a water redistribution model in a cracked vertisol at two scales. Vadose Zone J. 18, 1–11. https://doi.org/10.2136/vzj2018.09.0173.

Baram, S., Ronen, Z., Kurtzman, D., Külls, C., Dahan, O., 2013. Desiccation-crack-induced salinization in deep clay sediment. Hydrol. Earth Syst. Sci. 17, 1533–1545. https://doi.org/10.5194/hess-17-1533-2013.

Beven, K., Germann, P., 1982. Macropores and water flow in soils. Water Resour. Res. 18, 1311–1325. https://doi.org/10.1029/WR018i005p01311.

Bogaard, T.A., Greco, R., 2015. Landslide hydrology: from hydrology to pore pressure. WIREs Water. 3, 439–459. https://doi.org/10.1002/wat2.1126.

Caris, J.P.T., Van Asch, T.W.J., 1991. Geophysical, geotechnical and hydrological investigations of a small landslide in the French Alps. Eng. Geol. 31, 249–276. https://doi.org/10.1016/0013-7952(1)90011-9.

Chaduvula, U., Viswanadham, B.V.S., Kodikara, J., 2022. Centrifuge model studies on desiccation cracking behaviour of fiber-reinforced expansive clay. Geotext. Geomembr. 50, 480–497. https://doi.org/10.1016/j.geotexmem.2022.02.001.

Chen, C., Roseberg, R.J., Selker, J.S., 2002. Using microsprinkler irrigation to reduce leaching in a shrink/swell clay soil. Agric. Water Manage. 54, 159–171. https://doi.org/10.1016/s0378-3774(01)00150-0.

Chui, T.F.M., Freyberg, D.L., 2009. Implementing hydrologic boundary conditions in a multiphysics model. J. Hydrol. Eng. 14, 1374–1377. https://doi.org/10.1061/(asce)he.1943-5584.0000113.

Coppola, A., Gerke, H.H., Comegna, A., Basile, A., Comegna, V., 2012. Dual-permeability model for flow in shrinking soil with dominant horizontal deformation. Water Resour. Res. 48 https://doi.org/10.1029/2011wr011376.

Coppola, A., Comegna, A., Dragonetti, G., Gerke, H.H., Basile, A., 2015. Simulated preferential water flow and solute transport in shrinking soils. Vadose Zone J. 14 (9) https://doi.org/10.2136/vzj2015.02.0021.

Coumou, D., Rahmstorf, S., 2012. A decade of weather extremes. Nat. Clim. Change 2, 491–496. https://doi.org/10.1038/nclimate1452.

Davidson, M.R., 1984. A green-ampt model of infiltration in a cracked soil. Water Resour. Res. 20, 1685–1690. https://doi.org/10.1029/WR020i011p01685.

Gerke, H.H., Maximilian Köhne, J., 2004. Dual-permeability modeling of preferential bromide leaching from a tile-drained glacial till agricultural field. J. Hydrol. 289, 239–257. https://doi.org/10.1016/j.jhydrol.2003.11.019.

Gerke, H.H., Dusek, J., Vogel, T., 2013. Solute mass transfer effects in two-dimensional dual-permeability modeling of bromide leaching from a tile-drained field. Vadose Zone J. 12 (2) https://doi.org/10.2136/vzj2012.0091.

Gerke, H.H., van Genuchten, M.T., 1993. A dual-porosity model for simulating the preferential movement of water and solutes in structured porous media. Water Resour. Res. 29, 305–319. https://doi.org/10.1029/92wr02339.

Gerke, H.H., Dusek, J., Vogel, T., Köhne, J.M., 2007. Two-dimensional dual-permeability analyses of a bromide tracer experiment on a tile-drained field. Vadose Zone J. 6, 651–667. https://doi.org/10.2136/vzj2007.0033.

Greco, R., 2002. Preferential flow in macroporous swelling soil with internal catchment: model development and applications. J. Hydrol. 269, 150–168. https://doi.org/10.1016/s0022-1694(02)00215-9.

Greve, A., Andersen, M.S., Acworth, R.I., 2010. Investigations of soil cracking and preferential flow in a weighing lysimeter filled with cracking clay soil. J. Hydrol. 393, 105–113. https://doi.org/10.1016/j.jhydrol.2010.03.007.

Gui, Y.L., Zhao, Z.Y., Kodikara, J., Bui, H.H., Yang, S.Q., 2016. Numerical modelling of laboratory soil desiccation cracking using UDEC with a mix-mode cohesive fracture model. Eng. Geol. 202, 14–23. https://doi.org/10.1016/j.enggeo.2015.12.028.

Hirobe, S., Oguni, K., 2016. Coupling analysis of pattern formation in desiccation cracks. Comput. Methods Appl. Mech. Eng. 307, 470–488. https://doi.org/10.1016/j.cma.2016.04.029.

Jamalinia, E., Vardon, P.J., Steele-Dunne, S.C., 2020. The impact of evaporation induced cracks and precipitation on temporal slope stability. Comput. Geotech. 122, 103506.

Jarvis, N., Koestel, J., Larsbo, M., 2016. Understanding preferential flow in the vadose zone: recent advances and future prospects. Vadose Zone J. 15 (12) https://doi.org/10.2136/vzj2016.09.0075.

Khan, M.S., Hossain, S., Ahmed, A., Faysal, M., 2017. Investigation of a shallow slope failure on expansive clay in Texas. Eng. Geol. 219, 118–129. https://doi.org/10.1016/j.enggeo.2016.10.004.

Kroes, J.G., Wesseling, J.G., Van Dam, J.C., 2000. Integrated modelling of the soil – water – atmosphere – plantsystem using the model SWAP 2.0 an overview of theory andan application. Hydrol. Processes 14, 10. https://doi.org/10.1002/1099-1085(20000815/30)14:11/12<1993::AID-HYP50>3.0.CO;2-%23.

Larsbo, M., Jarvis, N. J., 2003. MACRO5.0. A model of water flow and solute transport in macroporous soil. Technical description.

Lepore, B.J., Morgan, C.L.S., Norman, J.M., Molling, C.C., 2009. A Mesopore and Matrix infiltration model based on soil structure. Geoderma 152, 301–313. https://doi.org/10.1016/j.geoderma.2009.06.016.

Lin, H., Zhou, X., 2007. Evidence of subsurface preferential flow using soil hydrologic monitoring in the Shale Hills catchment. Eur. J. Soil Sci. 59, 34–49. https://doi.org/10.1111/j.1365-2389.2007.00988.x.

Luo, Y.i., Zhang, J.-M., Zhou, Z., Shen, Z.-J., Chong, L., Victor, C., 2021. Investigation and prediction of water infiltration process in cracked soils based on a full-scale model test. Geoderma 400, 115111.

Luo, Y., Zhang, J., Zhou, Z., Aguilar-Lopez, J.P., Greco, R., Bogaard, T., 2023. Effects of dynamic changes of desiccation cracks on preferential flow: experimental investigation and numerical modeling. Hydrol. Earth Syst. Sci. 27, 26. https://doi.org/10.5194/hess-27-783-2023.

Mooney, S.J., Morris, C., 2008. A morphological approach to understanding preferential flow using image analysis with dye tracers and X-ray Computed Tomography. Catena 73, 204–211. https://doi.org/10.1016/j.catena.2007.09.003.

Morales, S.R., Lemon, M.G.T., Stewart, R.D., Keim, R.F., 2021. Flood-induced recharge of matrix water in a vertic forest soil. Water Resour. Res. 57 https://doi.org/10.1029/2021wr029675.

Mualem, Y., 1976. A new model for predicting the hydraulic conductivity of unsaturated porous media. Water Resour. Res. 12, 513–522. https://doi.org/10.1029/WR012i003p00513.

Neely, H.L., Ackerson, J.P., Morgan, C.L.S., McInnes, K.J., 2014. Instrumentation to measure soil subsidence and water content in a single borehole. Soil Sci. Soc. Am. J. 78, 1251–1257. https://doi.org/10.2136/sssaj2014.02.0055n.

Neely, H.L., Morgan, C.L.S., McInnes, K.J., Molling, C.C., 2018. Modeling soil crack volume at the pedon scale using available soil data. Soil Sci. Soc. Am. J. 82, 734–743. https://doi.org/10.2136/sssaj2018.01.0007.

Nimmo, J.R., 2010. Theory for source-responsive and free-surface film modeling of unsaturated flow. Vadose Zone J. 9, 295–306. https://doi.org/10.2136/vzj2009.0085.

Nimmo, J.R., Perkins, K.S., Plampin, M.R., Walvoord, M.A., Ebel, B.A., Mirus, B.B., 2021. Rapid-response unsaturated zone hydrology: small-scale data, small-scale theory. Big Problems. Front. Earth Sci. 9 https://doi.org/10.3389/feart.2021.613564.

Pei, P., Zhao, Y., Ni, P., Mei, G., 2020. A protective measure for expansive soil slopes based on moisture content control. Eng. Geol. 269, 105527.

Sánchez, M., Manzoli, O.L., Guimarães, L.J.N., 2014. Modeling 3-D desiccation soil crack networks using a mesh fragmentation technique. Comput. Geotech. 62, 27–39. https://doi.org/10.1016/j.compgeo.2014.06.009.

Shao, W., Bogaard, T.A., Bakker, M., Greco, R., 2015. Quantification of the influence of preferential flow on slope stability using a numerical modelling approach. Hydrol. Earth Syst. Sci. 19, 2197–2212. https://doi.org/10.5194/hess-19-2197-2015.

Shin, H., Santamarina, J.C., 2011. Desiccation cracks in saturated fine-grained soils: particle-level phenomena and effective-stress analysis. Géotechnique 61, 961–972. https://doi.org/10.1680/geot.8.P.012.

Sima, J., Jiang, M., Zhou, C., 2014. Numerical simulation of desiccation cracking in a thin clay layer using 3D discrete element modeling. Comput. Geotech. 56, 168–180. https://doi.org/10.1016/j.compgeo.2013.12.003.

Šimůnek, J., Jarvis, N.J., van Genuchten, M.T., Gärdenäs, A., 2003. Review and comparison of models for describing non-equilibrium and preferential flow and transport in the vadose zone. J. Hydrol. 272, 14–35. https://doi.org/10.1016/s0022-1694(02)00252-4.

Smith, R.J., Raine, S.R., Minkevich, J., 2005. Irrigation application efficiency and deep drainage potential under surface irrigated cotton. Agric. Water Manage. 71, 117–130. https://doi.org/10.1016/j.agwat.2004.07.008.

Stewart, R.D., 2018. A dynamic multidomain green-ampt infiltration model. Water Resour. Res. 54, 6844–6859. https://doi.org/10.1029/2018wr023297.

Stewart, R.D., 2019. A generalized analytical solution for preferential infiltration and wetting. Vadose Zone J. 18, 1–10. https://doi.org/10.2136/vzj2018.08.0148.

Stewart, R.D., Rupp, D.E., Abou Najm, M.R., Selker, J.S., 2016a. A unified model for soil shrinkage, subsidence, and cracking. Vadose Zone J. 15, 1–15. https://doi.org/10.2136/vzj2015.11.0146.

Stewart, R.D., Abou Najm, M.R., Rupp, D.E., Selker, J.S., 2016b. Modeling multidomain hydraulic properties of shrink-swell soils. Water Resour. Res. 52, 7911–7930. https://doi.org/10.1002/2016wr019336.

Tang, C.-S., Cui, Y.-J., Shi, B., Tang, A.-M., Liu, C., 2011. Desiccation and cracking behaviour of clay layer from slurry state under wetting–drying cycles. Geoderma 166, 111–118. https://doi.org/10.1016/j.geoderma.2011.07.018.

Tang, C.-S., Zhu, C., Cheng, Q., Zeng, H., Xu, J.-J., Tian, B.-G., Shi, B., 2021. Desiccation cracking of soils: a review of investigation approaches, underlying mechanisms, and influencing factors. Earth Sci. Rev. 216, 103586.

Tian, B.-G., Cheng, Q., Tang, C.-S., Zeng, H., Xu, J.-J., Shi, B., 2022. Effects of compaction state on desiccation cracking behaviour of a clayey soil subjected to wetting-drying cycles. Eng. Geol. 302, 106650.

Tran, K.M., Bui, H.H., Sánchez, M., Kodikara, J., 2020. A DEM approach to study desiccation processes in slurry soils. Comput. Geotech. 120, 103448.

van Genuchten, M.T., 1980. A closed-form equation for predicting the hydraulic conductivity of unsaturated soils. Soil Sci. Soc. Am. J. 44, 892–898. https://doi.org/10.2136/sssaj1980.03615995004400050002x.

Vo, T.D., Pouya, A., Hemmati, S., Tang, A.M., 2017. Numerical modelling of desiccation cracking of clayey soil using a cohesive fracture method. Comput. Geotech. 85, 15–27. https://doi.org/10.1016/j.compgeo.2016.12.010.

Weiler, M., 2005. An infiltration model based on flow variability in macropores: development, sensitivity analysis and applications. J. Hydrol. 310, 294–315. https://doi.org/10.1016/j.jhydrol.2005.01.010.

Wijerathne, M.L.L., Oguni, K., Hori, M., 2009. Numerical analysis of growing crack problems using particle discretization scheme. Int. J. Numer. Methods Eng. 80, 46–73. https://doi.org/10.1002/nme.2620.

Wilson, G.W., Fredlund, D.G., Barbour, S.L., 1997. The effect of soil suction on evaporative fluxes from soil surfaces. Can. Geotech. J. 34, 145–155. https://doi.org/10.1139/t96-078.

Xie, C., Ni, P., Xu, M., Mei, G., Zhao, Y., 2020. Combined measure of geometry optimization and vegetation for expansive soil slopes. Comput. Geotech. 123, 103588.

Xu, J.-J., Tang, C.-S., Cheng, Q., Vahedifard, F., Liu, B., Shi, B., 2022. Monitoring and early detection of soil desiccation cracking using distributed fibre optical sensing. Géotechnique 1–12. https://doi.org/10.1680/jgeot.21.00397.

Zeng, H., Tang, C.S., Zhu, C., Cheng, Q., Lin, Z.Z., Shi, B., 2021. Investigating soil desiccation cracking using an infrared thermal imaging technique. Water Resour. Res. 58 https://doi.org/10.1029/2021wr030916.

Zhang, J., Luo, Y., Zhou, Z., Victor, C., Duan, M., 2021a. Research on the rainfall-induced regional slope failures along the Yangtze River of Anhui, China. Landslides 18, 1801–1821. https://doi.org/10.1007/s10346-021-01623-7.

Zhang, J., Luo, Y., Zhou, Z., Chong, L., Victor, C., Zhang, Y., 2021b. Effects of preferential flow induced by desiccation cracks on slope stability. Eng. Geol. 288 https://doi.org/10.1016/j.enggeo.2021.106164.